Scaling of Unitary Synaptic Strength In the Context of Network Dynamics

by

Nathan R. Wilson

B.S., Biology
M.Eng., Computer Science
Cornell University, 2000

Submitted to the Department of Brain and Cognitive Sciences
in Partial Fulfillment of the Requirements for the Degree of

DOCTOR OF PHILOSOPHY

at the

MASSACHUSETTS INSTITUTE OF TECHNOLOGY

Cambridge, Massachusetts, USA

September 2005

Signature of Author _____
Department of Brain and Cognitive Sciences
September 2, 2005

Certified by _____
Dr. Guosong Liu
Edward J. Poitras Associate Professor of Neuroscience
Thesis Supervisor

Accepted by _____
Dr. Earl K. Miller
Picower Professor of Neuroscience
Chairman, Department Graduate Committee

SCALING OF UNITARY SYNAPTIC STRENGTH IN THE CONTEXT OF NETWORK DYNAMICS

by

NATHAN R. WILSON

Submitted to the Department of Brain and Cognitive Sciences on July 7, 2005
in Partial Fulfillment of the Requirements for the Degree of Doctor of Philosophy in
Brain and Cognitive Sciences

ABSTRACT

A fundamental consideration in understanding neuronal networks is determining what sets the unitary functional strength of a synaptic connection between two cells, and what meta-processes such mechanisms answer to. This question can be asked either mechanistically, by characterizing the molecular processes that regulate the synapse's transmission, or ontologically, by considering the impact of this transmission from the standpoint of neighboring synapses, the postsynaptic cell itself, or the network of neurons in which it is situated. The work presented here practices both approaches, by identifying a new molecular mechanism to which the quantal size of excitatory synapses can be attributed, and then beginning to explore how quantal size might be influenced by network activity and architecture.

Chapter 1 identifies a new molecular control point for specifying the quantal size of excitatory transmission in the mammalian brain, and provides the first known demonstration that such specification can be provided by a presynaptic process. It then details how this mechanism is regulated by network activity.

Chapter 2 makes use of a new methodology for designing the physical structure of cultured networks in order to begin to perturb network parameters and explore the role of quantal size in a network context. Applying this methodology I demonstrate that the quantal size of excitatory synapses is scaled by neurons inversely with their number of synaptic connections, and identify a set of mechanisms by which network firing is maintained at a constant level when the number of active synaptic partners is scaled.

Chapter 3 demonstrates progress towards a methodology capable of producing and detecting changes in the unitary strength of multiple synapses with respect to one another within a dendritic tree. Future efforts can hopefully make use of similar principles to directly visualize how heterosynaptic processes establish and maintain a contrast in the strengths of unitary synapses to enable representation by synaptically-based memory traces.

TABLE OF CONTENTS

ACKNOWLEDGEMENTS

CHAPTER 1

Presynaptic Regulation of Quantal Size by the Vesicular Glutamate Transporter VGLUT1

SUMMARY

A fundamental question in synaptic physiology is whether the unitary strength of a synapse can be regulated by presynaptic characteristics, and if so, what those characteristics might be. Here we characterize a newly proposed mechanism for altering the strength of glutamatergic synapses, based on the recently identified vesicular glutamate transport protein (VGLUT1). We provide direct evidence that filling in isolated synaptic vesicles is subject to a dynamic equilibrium that is determined by both the concentration of available glutamate and the number of vesicular transporters participating in loading. We observe that changing the number of vesicular transporters expressed at hippocampal excitatory synapses results in enhanced evoked and miniature responses, and verify biophysically that these changes correspond to an increase in the amount of glutamate released per vesicle into the synaptic cleft. Further, we find that this modulation of synaptic strength by vesicular transporter expression is endogenously regulated, both across development to coincide with a maturational increase in vesicle cycling and quantal amplitude, and by excitatory and inhibitory receptor activation in mature neurons to provide an activity-dependent scaling of quantal size via a presynaptic mechanism. Together, these findings underscore that vesicular transporter expression is utilized endogenously to directly regulate the extent of glutamate release, providing a concise presynaptic mechanism for controlling the quantal efficacy of excitatory transmission during synaptic refinement and plasticity.

INTRODUCTION

A continuing goal of synaptic physiology is to uncover the features of synaptic structure that most dramatically influence synaptic strength. In excitatory glutamatergic synapses, remarkable progress has been made in detailing the postsynaptic factors that regulate synaptic efficacy (Malenka and Nicoll, 1999; Sheng and Kim, 2002). However, comparatively less has been done to identify corresponding presynaptic mechanisms that influence postsynaptic activation by governing the amount of transmitter released (Atwood and Karunanithi, 2002; Liu, 2003). Nevertheless, recent studies at central synapses have demonstrated that normal transmitter release can be insufficient to fully activate postsynaptic receptors (Bekkers et al., 1990; Liu and Tsien, 1995; Silver et al.,

1996; Forti et al., 1997; Liu et al., 1999; Mainen et al., 1999; McAllister and Stevens, 2000), and variability in excitatory quantal size is increasingly considered to be largely attributable to presynaptic fluctuations in transmitter release (Liu et al., 1999; Hanse and Gustafsson, 2001; Franks et al., 2003). It is thus worthwhile to consider what presynaptic molecular mechanisms might influence the amount of glutamate released into the synaptic cleft, and whether such mechanisms might be endogenously controlled to provide additional modes of synaptic regulation.

Recent work has demonstrated that artificial perturbations can alter excitatory transmission by modulating the amount of glutamate released from synaptic vesicles. In particular, either disrupting electrochemical proton gradients that drive the loading of transmitter into vesicles prior to release (Zhou et al., 2000) or making additional glutamate available for loading (Ishikawa et al., 2002; Yamashita et al., 2003) are both effective at changing the degree of postsynaptic activation during transmission.

We hypothesize that postsynaptic activation is similarly controlled by endogenous presynaptic mechanisms, via the expression of the vesicular glutamate transporter VGLUT1 which is now known to underlie the transport of glutamate into excitatory vesicles (Bellocchio et al., 2000; Takamori et al., 2000). Functional work has recently demonstrated that perturbations to VGLUT1 expression can influence the strength of excitatory transmission, with knocking out VGLUT1 in particular leading to a profound reduction in excitatory signaling (Fremeau et al., 2004; Wojcik et al., 2004). VGLUT1 thus seems well-poised as a control point for regulating synaptic transmission, though its precise mode of action in synaptic transmission remains uncharacterized and its propensity for meaningful regulation is unreported. Indeed, though properties of cholinergic (Song et al., 1997) and aminergic (Pothos et al., 2000) vesicular transporters have now been examined as well, whether the expression of any vesicular transporter can be controlled endogenously to facilitate activity-dependent plasticity has not been explored.

The present work thus aims to 1) more fully characterize the manner by which VGLUT1 expression is able to influence synaptic function, and 2) elucidate whether neurons actually make use of this machinery endogenously, to presynaptically modulate the function of excitatory signaling. The characterizations of VGLUT1 described below, along with the specific expression of VGLUT1 in brain areas associated with adult plasticity (Fremeau et al., 2001; Liu, 2003), suggest an intriguing role for the

regulation of vesicular transport in facilitating the functional dynamic range of glutamatergic synapses.

RESULTS

VGLUT1 Loading in Synaptic Vesicles Depends on Glutamate Concentration and Number of Available Transporters

To characterize the nature by which VGLUT1 expression might impact synaptic transmission, it was first important to demonstrate that varying the parameters of glutamate transport could actually modulate the extent of vesicle filling. A possible scenario is that while different transport conditions might influence the speed of filling, vesicles eventually fill to a "set point" that is dictated by some parameter independent of transport, such as vesicle size. On the other hand, if the amount of glutamate loaded into vesicles were to be specified by a dynamic equilibrium process that could be stoichiometrically influenced by the components of the loading reaction, it would allow for the modulation of vesicle filling and the consequent release of glutamate by endogenous characteristics such as transporter expression.

Previous work has assayed the loading of glutamate into PC12 cells (Bellocchio et al., 2000), BON cells (Takamori et al., 2000), and even purified synaptic vesicles at specific external glutamate concentrations (Maycox et al., 1988; Wolosker et al., 1996). However, given a recent set of insightful studies that has begun to elucidate the previously unknown range of the cytosolic glutamate concentration (Ishikawa et al., 2002; Yamashita et al., 2003), we were interested in systematically measuring the glutamate uptake equilibrium around variants of this physiological range of conditions, as well as assessing the influence of transporter number in defining this equilibrium.

We therefore quantified the time course and final equilibrium of glutamate transport under different conditions, using VGLUT1 synaptic vesicles isolated from rat cerebral cortex and hippocampus (Figure 1). Observing the vesicles' uptake of 50 μM ^{3}H-glutamate (Figure 1A) revealed that vesicular transport in our system reached an equilibrium balance between transmitter influx and efflux along a similar timecourse to that reported previously (Maycox et al., 1988; Wolosker et al., 1996). To examine whether the number of transporters participating in loading could influence its final equilibrium, we also compared our equilibrium uptake to that occurring in the presence

Figure 1. VGLUT1 Loading in Synaptic Vesicles Depends on Glutamate Concentration and Number of Available Transporters

(A) Uptake timecourse of 50 μM ^{3}H-glutamate by purified synaptic vesicles (●) reaches equilibrium in about 10 minutes. Uptake in the presence of either the competitive VGLUT1 inhibitor trypan blue (□) or the non-competitive VGLUT1 inhibitor rose bengal (o) both fill along a similar timecourse, but to smaller equilibrium amounts.

(B) Uptake timecourse for 1 mM ^{3}H-glutamate by synaptic vesicles (●) occurs along a similar timecourse as in (A), but to a dramatically increased final equilibrium amount. Equilibrium is again reduced in the presence of either trypan blue (□) or rose bengal (o).

(C) Saturation isotherm of ^{3}H-glutamate (0.06 - 6 mM) accumulation at 10 min in the presence and absence of rose bengal (o) or trypan blue (□). In the presence of >1 mM glutamate, the competitive trypan blue inhibition is lost while the non-competitive rose bengal inhibition is maintained.

(D) Time courses of ^{3}H-glutamate uptake at four sub-saturating concentrations of glutamate show that steady-state vesicular glutamate levels depend on the concentration of glutamate present in the medium.

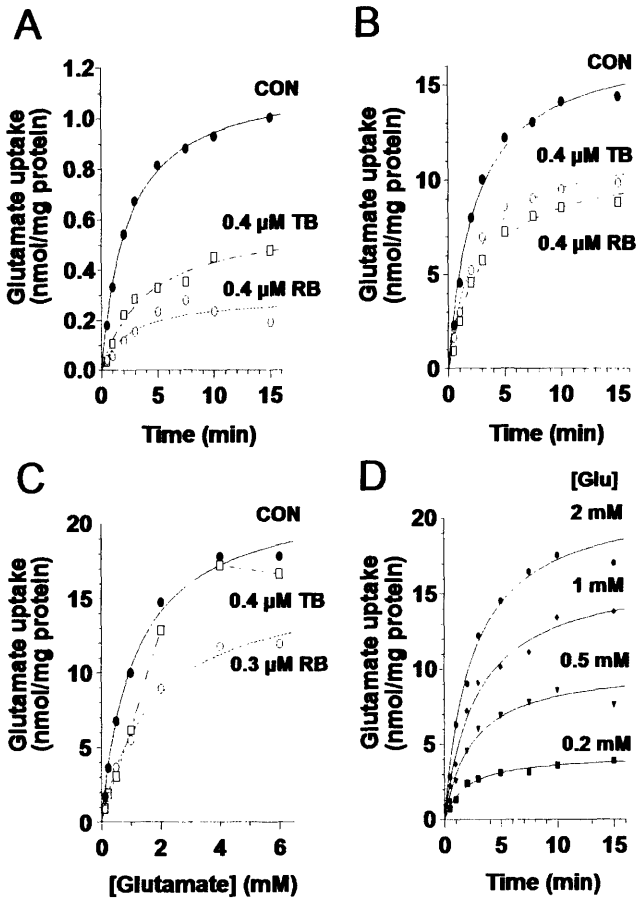
A
Glutamate uptake (nmol/mg protein)
CON
0.4 μM TB
0.4 μM RB
Time (min)
B
Glutamate uptake (nmol/mg protein)
CON
0.4 μM TB
0.4 μM RB
Time (min)
C
Glutamate uptake (nmol/mg protein)
CON
0.4 μM TB
0.3 μM RB
[Glutamate] (mM)
D
Glutamate uptake (nmol/mg protein)
[Glu]
2 mM
1 mM
0.5 mM
0.2 mM
Time (min)

of rose bengal (RB), an antagonist of VGLUT1 loading that is believed to interact allosterically with the transporter (Ogita et al., 2001). Since the drug is thought to non-competitively disrupt glutamate transport at the site of loading, it offered a pharmacological means for reducing the effective number of transporters participating in uptake, in order to examine whether the size of the available transporter pool can help determine the final amount of vesicle filling. Loading in the presence of rose bengal indeed exhibited a reduced equilibrium of filling (Figure 1A), a property that was also observed under treatment with trypan blue (TB), the most potent known competitive antagonist of vesicular glutamate transport (Roseth et al., 1998). Both drugs were applied at approximate IC50 concentrations, whereby 2 μM at either 5 or 10 minute pre-incubation achieved complete inhibition of loading (data not shown).

By repeating these treatments under a more physiological concentration of extravesicular glutamate (1 mM, Figure 1B), we were next able to observe whether transporter activity can also influence vesicle filling at a glutamate concentration closer to what has endogenously been estimated in functional studies (Ishikawa et al., 2002). At this higher concentration of glutamate, the vesicles now filled to a higher steady-state concentration, indicating that the final extent of VGLUT1 filling depends directly upon the concentration of glutamate around the vesicle, and does not have an independent set point. Equilibrium filling was again reduced by the presence of either RB or TB (Figure 1B) demonstrating that also at this higher concentration the equilibrium can be shifted by reducing the number of active transporters contributing to the loading process.

Varying the external glutamate concentration along a continuum while measuring 10 minute equilibrium uptake levels (Figure 1C) reveals that maximal uptake increases linearly up to 1 mM of exogenous glutamate and begins to saturate at approximately 4-6 mM. Even at these concentrations, the extent of transporter availability is critical in determining the equilibrium value, since RB attenuates the final concentration reached for all values of external glutamate in a similar manner to TB, though TB's competitive antagonism is eventually overwhelmed as glutamate concentration is increased. Taken together, the results lead us to conclude that VGLUT1 vesicles are subject to a flexible degree of filling that can be influenced by both the concentration of glutamate outside of the vesicle as well as the effective number of available transporters. Aligning the time courses of loading observed under

various glutamate concentrations (Figure 1D) demonstrates that both the magnitude and to a lesser degree the rate of uptake are influenced by alterations in transport conditions.

We thus observe three properties of glutamate uptake into synaptic vesicles at physiological terminal glutamate concentrations. First, further increases to external glutamate concentrations can enhance the amount of transmitter loaded, as predicted by the aforementioned functional work (Ishikawa et al., 2002; Yamashita et al., 2003). Second, the number of transporters available for loading can influence the final loading equilibrium, even at glutamate concentrations above the physiological range. Third, vesicle filling is a slow process, requiring minutes to reach completion, which could indicate an importance of changes to the vesicle loading *rate*, in addition to the loading *amount*, in determining physiological synaptic transmission.

Transporter Overexpression in PC12 Cells and Hippocampal Synapses

If VGLUT1 vesicles do not merely accumulate transmitter until full, but rather have their speed and amount of filling determined by an equilibrium process that is subject to the available concentration of transmitter and transporter, we were interested in examining whether this equilibrium could also be shifted in a more physiological context. We thus next attempted to vary the amount of vesicular transporters expressed in the synaptic terminals of neurons, to examine the resulting consequences for glutamate release in endogenous synaptic transmission.

To characterize the functional relationship between VGLUT1 expression and excitatory synaptic transmission, we attempted to over-express the transporter at hippocampal synaptic terminals. We created two expression constructs for delivery into neurons, one for wild-type VGLUT1 and another tagging VGLUT1 with the reporter green fluorescent protein (GFP) at its C-terminus. In order to verify the effectiveness of our constructs in enhancing VGLUT1 expression, PC12 cells were transiently transfected as previously described for VGLUT2 (Varoqui et al., 2002) and the recently identified VGLUT3 (Schafer et al., 2002). A Western blot analysis (Figure 2A) using a guinea pig antibody specific for VGLUT1 (Schafer et al., 2002), reveals that while mock-transfected cells (M) did not express detectable levels of VGLUT1, single immunoreactive bands of appropriate size were observed for PC12 cells transfected with either the wild-type VGLUT1 (WT) or the VGLUT-GFP fusion (+GFP) constructs. The fusion protein had an approximately 26 Kb higher molecular weight

Figure 2. Overexpression of VGLUT1 in PC12 Cells and Hippocampal Synapses

(A) Expression of both wild-type VGLUT1 (WT) and GFP-tagged VGLUT1 (+GFP) constructs in PC12 cells reveal single immunoreactive bands of appropriate size for wild-type and EGFP-tagged proteins as visualized by Western blot. Mock transfected cells (M) did not contain immunoreactivity.

(B) Both constructs succeeded in facilitating CCCP-sensitive glutamate loading into PC12 cells, whereas mock transfection did not.

(C) Top Panels: Overexpressed VGLUT1-GFP fusion protein localized to synaptic terminals (top) as shown by co-localization of the fusion protein (green) with FM4-64 (red). Scale bar: 10 μm. Bottom Panel: Wild-type VGLUT1 co-transfected with GFP clearly labels the morphology of transfected neurons.

(D) Double-immunostaining for synapsin I and VGLUT1 along GFP-labeled hippocampal axons. VGLUT1 intensity was higher in axons expressing GFP+VGLUT (top images) than in axons expressing GFP alone (bottom images).

(E) Ratio of VGLUT1 integrated optical density (IOD) to synapsin I IOD at individual synapses. Ratios were higher along axons transfected with GFP+VGLUT (left, 278 transfected synapses, 576 control synapses) than axons transfected with GFP alone or adjacent non-transfected synapses from the same area (right, 92 transfected synapses, 422 control synapses).

(F) Summary data across multiple cover slips (total n=8) for data in (E). GFP+VGLUT1 co-transfection results in augmented VGLUT1 protein levels per synapse.

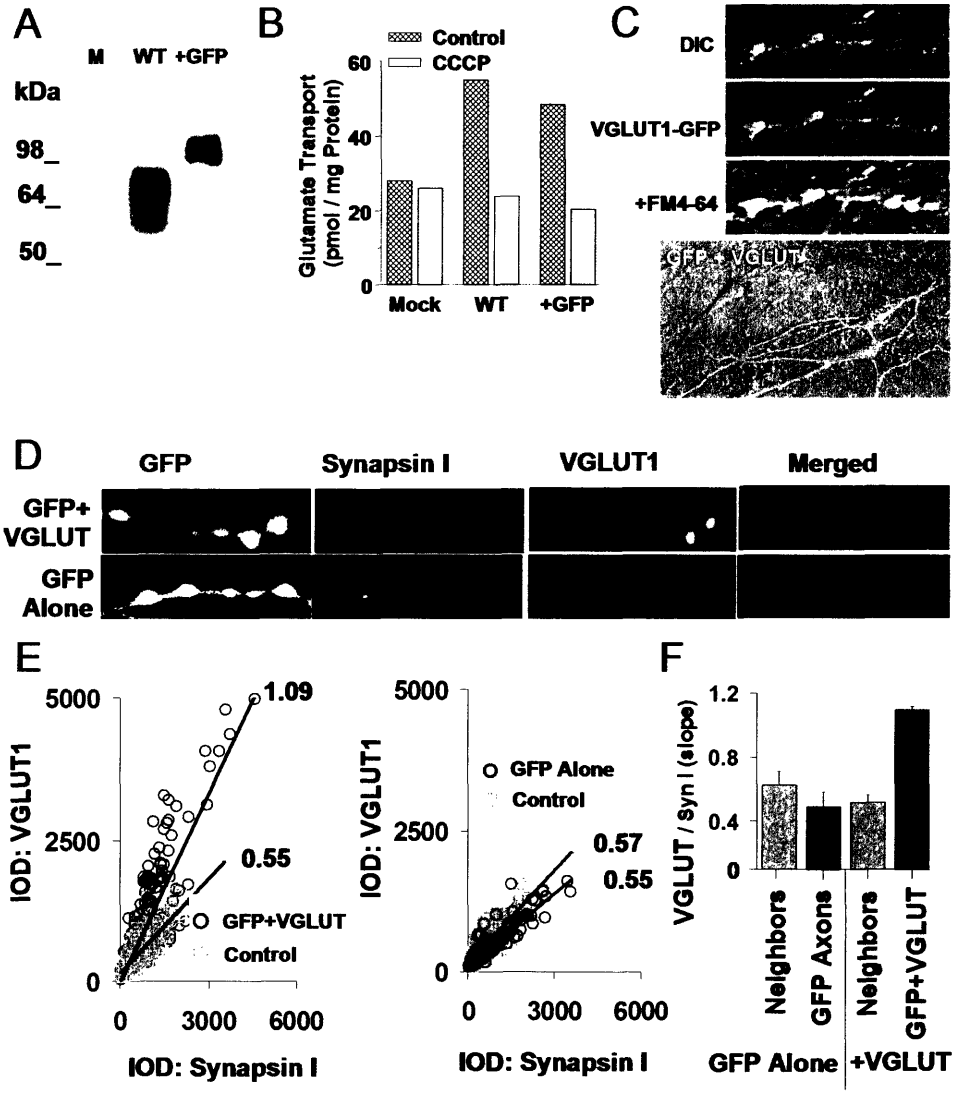
A
M
WT +GFP
kDa
98_
64_
50_
B
Control
CCCP
Glutamate Transport (pmol / mg Protein)
60
40
20
0
Mock
WT
+GFP
C
DIC
VGLUT1-GFP
+FM4-64
GFP + VGLUT
D
GFP
Synapsin I
VGLUT1
Merged
GFP+ VGLUT
GFP Alone
E
5000
2500
0
IOD: VGLUT1
1.09
0.55
GFP+VGLUT
Control
0
3000
6000
IOD: Synapsin I
GFP Alone
Control
0.57
0.55
F
VGLUT / Syn I (slope)
1.2
0.8
0.4
0
Neighbors
GFP Axons
Neighbors
GFP+VGLUT
GFP Alone
+VGLUT

than wild-type VGLUT1, due to the additional mass of the fused EGFP. To check the functionality of these newly synthesized proteins, we observed whether transfection of our constructs into PC12 cells gave rise to glutamate transport, by assaying for radioactive glutamate uptake in the presence of magnesium-ATP and chloride ions to activate transporter function (Figure 2B). Here, both wild-type VGLUT1 (WT) and GFP-tagged (+GFP) constructs demonstrated successful transport of ^{3}H-glutamate into a light population of membranes, a function that was found to be inhibited by the proton uncoupler carbonyl cyanide m-chlorophenylhydrazone (CCCP). CCCP-sensitive uptake in this and similar preparations of vesicles is considered a valid indicator of the H^{+}-dependent uptake of glutamate (Takamori et al., 2000; Takamori et al., 2002). While notable levels of uptake were not observed in mock-transfected cells (Mock), uptake capacity for both constructs were found to be comparable to those reported previously for VGLUT1 (Bellocchio et al., 2000; Takamori et al., 2000) as well as for VGLUT2 and VGLUT3 (Schafer et al., 2002; Varoqui et al., 2002). We therefore concluded that our constructs were effective at increasing VGLUT1 protein levels and enhancing glutamate transport.

We next examined whether VGLUT1 protein levels could be enhanced at the synaptic terminals of hippocampal neurons. This requires not only an increase in the production of VGLUT1 protein in transfected neurons, but also that the VGLUT1 generated from our constructs contain the correct targeting sequence to be transferred to synaptic terminals effectively. We examined VGLUT1 targeting by transfecting neurons with the VGLUT1-GFP fusion construct and visualizing protein localization. Here, confocal imaging of the fluorescent-tagged protein (Figure 2C, Top panels) showed that new protein was successfully targeted to the synaptic terminals, where it accumulated in discrete puncta co-localized with the presynaptic bouton label FM4-64, and was not observable in dendrites. In contrast, when GFP was co-transfected separately from VGLUT1 to fully label neurons overexpressing the protein for later experiments (Figure 2C, Bottom panel), the GFP diffused evenly throughout the cell, with no specific targeting to synaptic terminals. We therefore conclude that overexpressed VGLUT1 can be targeted to hippocampal synapses.

Though the fusion construct proved useful for establishing the targeting of overexpressed protein to synaptic terminals, we chose to use wild-type VGLUT1 for the subsequent functional characterizations to avoid any modification of VGLUT1 structure

that could perturb insertion at the vesicular membrane or disrupt potential endogenous regulation at the terminal. It was then necessary to verify that our VGLUT1 / GFP co-transfection also succeeded in increasing total VGLUT1 protein levels at the synaptic terminal. Figure 2D shows immunolabeled VGLUT1 occurring within synaptic terminals marked with synapsin I along axons co-transfected with GFP and VGLUT1 (top images), or transfected with GFP alone (bottom images). We found that VGLUT1 puncta appeared more intense in synapses occurring on the GFP-labeled transfected axon than in neighboring puncta occurring off of the GFP axon (top images). As an additional control demonstrating that GFP transfection alone did not enhance VGLUT1 levels per synaptic terminal, the above comparison was repeated with GFP axons lacking VGLUT1 co-transfection, again vs. neighboring GFP-negative terminals (Figure 2D, Bottom images). In this case, there did not appear to be an appreciable difference in the size or intensities of VGLUT1 puncta occurring on or off of the GFP-labeled axon.

The absolute amount of VGLUT1 per synapse is determined by both the number of synaptic vesicles and the average amount of VGLUT1 protein per vesicle. It was important to discern whether any increase in VGLUT1 levels that we observed was indeed due to a specific change in the concentration of VGLUT1 across the synapse, and not just a general increase in the size or density of the vesicle pool. Since synapsin I intensity provides a measure of the concentration of a second protein associated with vesicles, we used the ratio of VGLUT1 to synapsin I to determine the available amount of transporter protein independently of fluctuations in the number of vesicles or the synaptic area. Figure 2E demonstrates a quantification of this measure, which utilizes the integrated optical density (IOD) of VGLUT1 and synapsin I to compare the expression levels of the two proteins. Synapses from "GFP+VGLUT" axons show a nearly two-fold increase in the VGLUT1 / synapsin I IOD ratio compared to neighboring synaptic terminals (left plot). "GFP alone" axons, on the other hand, did not show noticeably larger VGLUT1 / synapsin I IOD ratios than in neighboring terminals (right plot). Repeating this measure across multiple cover slips demonstrates a consistent increase in the targeting of VGLUT1 protein to synapses as a result of GFP+VGLUT1 co-transfection (Figure 2F), with no increase in VGLUT1 protein at neighboring synapses in the same neuronal network. We therefore conclude that our constructs were capable of effectively targeting elevated levels of VGLUT1 protein to the synaptic terminals of our hippocampal cultures.

VGLUT1 Overexpression Enhances AMPA Receptor-Mediated Responses and Decreases Evoked Failure Rate

Having demonstrated a successful elevation of VGLUT1 protein levels in synaptic terminals, we examined the physiological consequences for functional synaptic transmission. Traditional electrophysiological methods record events postsynaptically, such that postsynaptic genetic manipulations have the possibility of influencing all recorded events. Presynaptic modifications, however, are more difficult to assay, as they require strict differentiation over which terminals are contributing to measured events. To solve this problem, we employed dual whole cell patch clamp, evoking an action potential in a presynaptic cell under current clamp while recording the resulting excitatory postsynaptic currents (EPSCs) mediated by α-amino-3-hydroxy-5-methyl-4-isoxazolepropionic acid (AMPA) receptors in a neighboring postsynaptic cell under voltage clamp (Figure 3A, Traces). Using confocal microscopy (Figure 3A, Image), we could distinguish presynaptic cells that were transfected with VGLUT1 by their co-expressed GFP label, as opposed to control neurons that did not express GFP. A common paradigm was to elicit transmission from a VGLUT1 neuron to a control neuron, and then as an independent control evoke synaptic transmission under reverse configuration to compare reciprocal transmission. Figure 3B shows evoked synaptic transmission in a reciprocally-connected pair of neurons (Top), where stimulating a "VGLUT-enhanced" neuron evoked an EPSC that was an average of 92% larger than that evoked from the control neuron in the reverse direction (left traces). Normalizing these traces to the same peak amplitude (right traces) revealed a similar average time course. Visualizing the distribution of events evoked from this reciprocal pair (Figure 3C) reveals a rightward shift in the VGLUT+ distribution relative to Control ($P < 0.0001$, Kolmogorov-Smirnov test), and on average control events were consistently exceeded by their VGLUT+ counterparts in EPSC amplitude (12.5 ± 2.9 vs. 20.5 ± 3.4, respectively; $P < 0.05$ unpaired t-test; $n = 7$ pairs Control; 7 pairs VGLUT+; Figures 3D).

Of potential interest, VGLUT+ transmission also exhibited an unexpected decrease in the failure rate of synaptic transmission (0.54 ± 0.11 vs. 0.18 ± 0.13, respectively; $P = 0.03$ unpaired t-test; Figures 3E), suggesting that transporter overexpression leads to an increase in either 1) the number of release events that are

Figure 3. Enhanced Excitatory Synaptic Transmission via VGLUT1 Overexpression
(A) Experimental paradigm: Dual whole cell patch clamp is achieved between a VGLUT1+GFP overexpressing "VGLUT+" neuron (green) and a non-transfected "Control" neuron (clear). An action potential is evoked in one neuron of the pair under current clamp at 0.3 Hz and the resulting excitatory postsynaptic current (EPSC) is recorded in the other neuron under voltage clamp. Scale Bars: 50 pA, 50 ms.
(B) EPSC responses evoked in a reciprocally-connected pair of "VGLUT+" and "Control" neurons. Average EPSCs (left traces) contrast the responses evoked from each type of presynaptic neuron. Scale Bars: 10 pA, 20 ms. Normalizing these traces to the same peak amplitude (right traces) reveals a similar time course.
(C) Distribution of EPSC amplitudes observed in the reciprocal pair shown in **(B)**. Events from a VGLUT+ presynaptic neuron tend to comprise a right-shifted distribution that differs in shape from its control counterpart.
(D) Summary data for the effect of presynaptic VGLUT1 overexpression on EPSC amplitude: mean amplitude measured across multiple pairs is significantly higher for VGLUT+ (*, $P < 0.05$ unpaired t-test; $n = 7$ Control, $n = 7$ VGLUT+).
(E) Summary data for the effect of overexpression on failure rate of evoked transmission: probability of receiving a postsynaptic response to presynaptic stimulation is increased by VGLUT1 overexpression (*, $P = 0.03$ unpaired t-test).

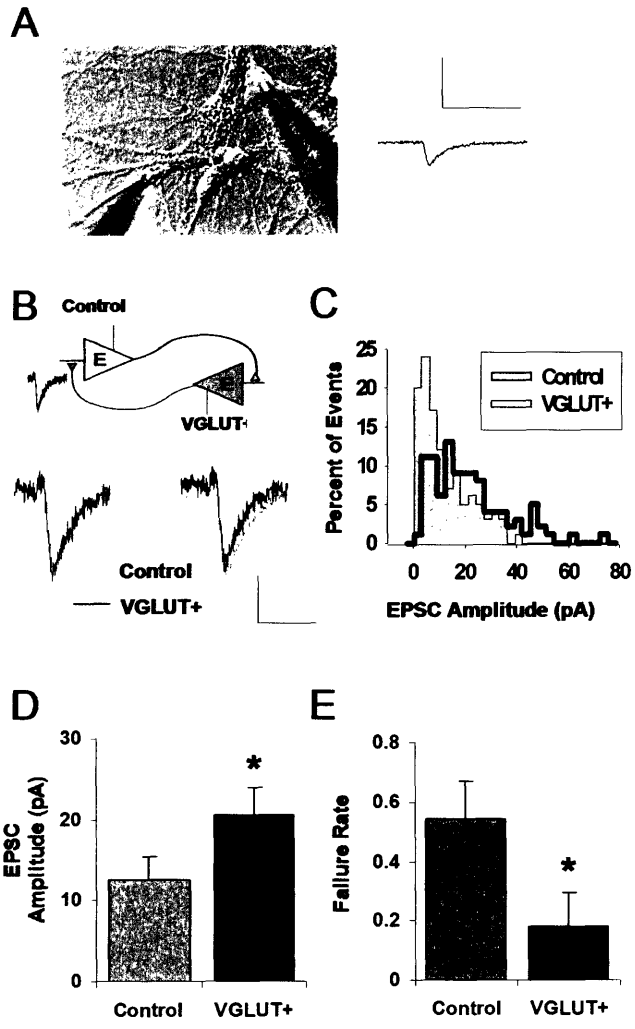
A
B
Control
E
VGLUT+
Control
VGLUT+
C
Control
VGLUT+
Percent of Events
25
20
15
10
5
0
0
20
40
60
80
EPSC Amplitude (pA)
D
EPSC Amplitude (pA)
30
20
10
0
*
Control
VGLUT+
E
Failure Rate
0.8
0.6
0.4
0.2
0
*
Control
VGLUT+

large enough to elicit detectable AMPA receptor-mediated responses, 2) the probability that a vesicle will be released following an action potential.

VGLUT1 Overexpression Enhances Quantal Synaptic Transmission

Increases in evoked synaptic transmission after VGLUT1 overexpression could be due to changes in the number of synaptic terminals, the probability of release per terminal, or the individual quantal size of response following each release. We thus next examined whether quantal transmission is impacted by VGLUT1 overexpression, by monitoring miniature synaptic transmission under bath application of tetrodotoxin to block action potentials and ensure spontaneous, single-vesicle release in Control vs. VGLUT1-overexpressing neurons. The difficulty in interpreting this experiment, of course, is that not all presynaptic terminals in a recorded neuron can be successfully transfected. Our strategy then was to rely first on a high transfection rate (~25%) and from this population select areas of the cover slip unusually dense in transfected cells and their axons (Figure 4A, Bottom image). Under this condition, for a given recorded neuron, a perceptible proportion of presynaptic terminals should contain higher levels of VGLUT1. Comparing responses observed here ("VGLUT+") to responses collected in a completely non-transfected cover slip ("Control"), we attempted to assay for detectable changes in quantal transmission.

mEPSCs recorded from neurons in areas rich in VGLUT+ terminals were larger than those recorded in cells devoid of enhanced terminals. Comparing distributions from sample VGLUT+ and Control neurons indicated a rightward shift of amplitudes in the VGLUT+ cultures (Figure 4B, $P < 0.001$, Kolmogorov-Smirnov test), while aligning sample and average traces (Figure 4C) further emphasized the difference. On average, the size of mEPSCs from the neurons with VGLUT1 transfection was 31% larger than that of neurons in the control group (13.6 ± 0.6 vs. 17.8 ± 2.2, respectively; $P = 0.04$ unpaired t-test; $n = 5$ cells Control; 8 cells VGLUT+; Figures 4D). In Figure 4D we also compared the effects of VGLUT transfection in miniature vs. evoked synaptic transmission. "Control" mEPSCs and EPSCs were similar in amplitude, suggesting that evoked EPSCs most likely originated from single synapses. Interestingly, while EPSCs evoked from transfected terminals were 64% larger than control, VGLUT+ mEPSCs only increased by 31%. This difference is expected from

Figure 4. Effects of VGLUT1 Overexpression on Quantal Excitatory Transmission

(A) mEPSCs were recorded postsynaptically via whole cell patch clamp in the presence of TTX in either a network completely lacking VGLUT1 overexpression ("Control") or from a sub-region of a transfected network visually determined to be dense in overexpressing neurons ("VGLUT+").

(B) Distributions of mEPSC amplitudes observed in the neurons shown in (A). VGLUT+ events tend to be right-shifted relative to the Control event distribution.

(C) Sample mEPSCs from cells recorded in Control and VGLUT+, which in this case are an average of 48% larger in the VGLUT+ recording. Scale Bars: 25 pA, 150 ms.

(D) Average mEPSC amplitude for neurons recorded in each group shows an increase in VGLUT+ mean event amplitude (*, $P = 0.04$ unpaired t-test). mEPSC data is aligned with the EPSC amplitude data from Figure 3C.

(E) No significant difference between Control and VGLUT+ neurons is observed for mEPSC frequency (shown), or rise and decay time kinetics (data not shown).

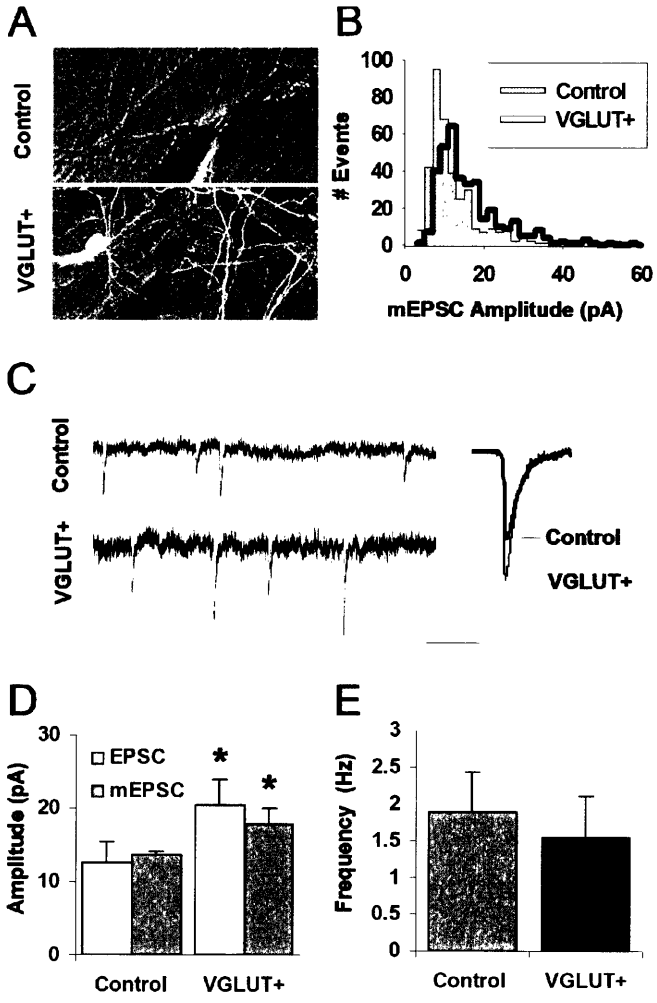
A
Control
VGLUT+
B
100
80
60
40
20
0
Events
Control
VGLUT+
0
20
40
60
mEPSC Amplitude (pA)
C
Control
VGLUT+
Control
VGLUT+
D
30
20
10
0
Amplitude (pA)
EPSC
mEPSC
*
*
Control
VGLUT+
E
3
2.5
2
1.5
1
0.5
0
Frequency (Hz)
Control
VGLUT+

the fact that the "VGLUT+" mean mEPSC amplitude was calculated from a population of events that included both VGLUT-enhanced and control terminals, and also given likely differences in detectability between evoked and spontaneous transmission (Zhou et al., 2000). Examining mEPSC frequency between the two pools of cells revealed no significant change (1.89 ± 0.54 vs. 1.55 ± 0.56, respectively; $P = 0.33$ unpaired t-test; Figure 4E). Similarly to what we observed in evoked transmission, no change was also observed in the time course of control and VGLUT-enhanced spontaneous transmission (data not shown), suggesting that VGLUT1 overexpression did not induce detectable changes in postsynaptic receptor properties.

VGLUT-Enhanced Transmission Results from Increased Glutamate Release per Vesicle

Changes in evoked and quantal transmission upon VGLUT1 overexpression could be due to either presynaptic changes in cleft glutamate concentration, or postsynaptic changes in receptor number or properties. We therefore next investigated whether the observed enhancement to evoked and miniature excitatory transmission following VGLUT1 overexpression was due to an increased amount of glutamate released from synaptic vesicles. To assess the extent of glutamate release during synaptic transmission, we made use of a previously established pharmacological approach (Liu et al., 1999; Wadiche and Jahr, 2001). The low-affinity antagonist γ-D-glutamylglycine (γ-DGG) competes with glutamate for postsynaptic AMPA receptors, such that it partially attenuates glutamatergic release events at hippocampal synapses. Due to the competitive nature of its interaction with glutamate, the degree of its attenuation is inversely related to the amount of glutamate being released, such that it can be used as a quasi-direct indicator of the extent of glutamate release (Liu et al., 1999). By recording EPSCs and determining the extent of γ-DGG attenuation, we could thus obtain a relative metric of the amount of glutamate involved in a population of synaptic release events.

We therefore repeated our dual whole cell patch clamp procedure (Figure 3), this time with perforated patches to obtain long-duration recordings. We evoked EPSCs from either Control or VGLUT-enhanced presynaptic neurons, and then applied γ-DGG to measure the impact of the antagonist on the transmission. By repeatedly evoking transmission at a regular interval, it was possible to establish a baseline amplitude that could then be reliably attenuated by the perfusion of 600 μM γ-DGG (Figure 5A), a

Figure 5. Enhanced Per Vesicle Glutamate Release via VGLUT1 Overexpression

(A) Sample application of the competitive glutamate antagonist γ-DGG (600 μM) while evoking EPSCs at 0.3 Hz between a pair of neurons. Dots represent an average of three EPSCs.

(B) Dose-response curve measuring the degree of EPSC attenuation by different concentrations of the competitive glutamate antagonist γ-DGG.

(C) Typical attenuation of Control vs. VGLUT-mediated EPSCs by 600 μM γ-DGG. Shown are median traces from single connections, normalized by pre-drug amplitudes for direct comparison. Lower traces depict the γ-DGG normalized to the height of their pre-drug counterpart for comparison of kinetics.

(D) Summary data of γ-DGG attenuation across all observed connections: VGLUT-mediated transmission is significantly less attenuated than control-mediated transmission (*, $P < 0.05$ unpaired t-test) ("Control" vs. "VGLUT+" bars). Also shown are summary data for γ-DGG attenuation acquired under intentionally reduced probability of release conditions ("Control, Low Pr" vs. "VGLUT+, Low Pr" bars – see Results). Here, VGLUT-mediated transmission is again significantly less attenuated than control-mediated transmission (*, $P < 0.05$ unpaired t-test). Average failure rates used during each condition are depicted in (F).

(E) Examples of tuning the failure rate of synaptic transmission by varying divalent cation concentrations, for "Low Pr" experimental conditions. The ratio of calcium / magnesium concentrations is varied while failure rate is measured until failure rate is sufficiently high to ensure a significant number of single vesicle events. Marker denotes condition where γ-DGG attenuation data was acquired.

(F) Average failure rates used during Normal Pr and "Low Pr" experiments summarized in (D). Failure rates were intentionally increased during the "Low Pr" experiments for both Control (*, $P < 0.05$ unpaired t-test) and VGLUT+ (**, $P < 0.01$ unpaired t-test) conditions.

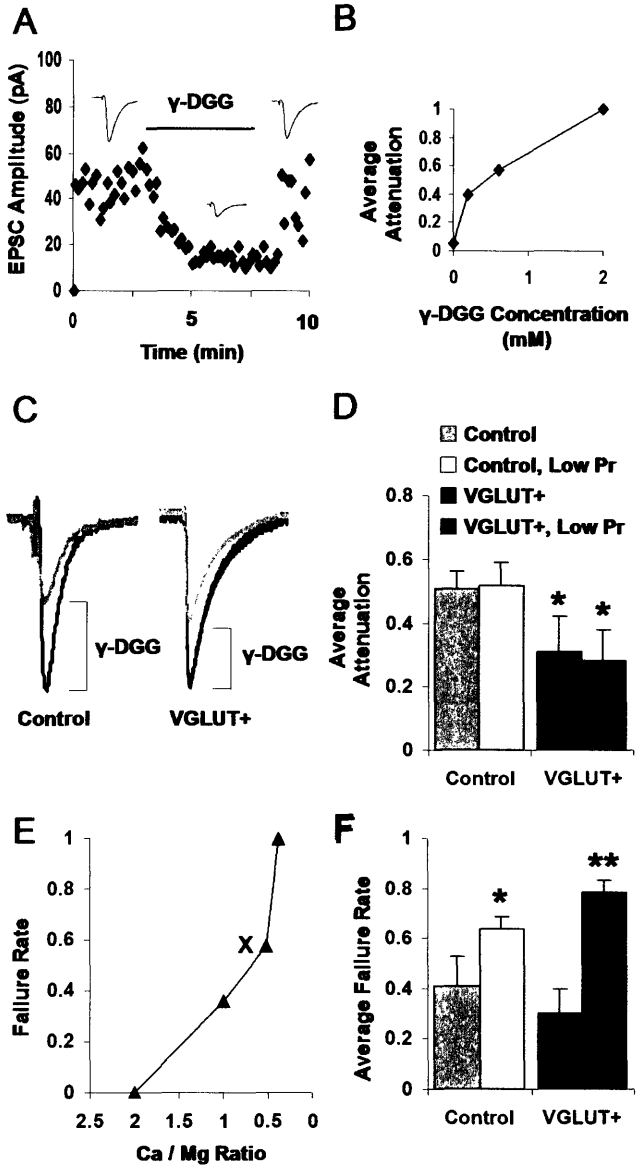
A
EPSC Amplitude (pA)
100
80
60
40
20
0
γ-DGG
0
5
10
Time (min)
B
Average Attenuation
1
0.8
0.6
0.4
0.2
0
0
1
2
γ-DGG Concentration (mM)
C
γ-DGG
γ-DGG
Control
VGLUT+
D
Control
Control, Low Pr
VGLUT+
VGLUT+, Low Pr
Average Attenuation
0.8
0.6
0.4
0.2
0
*
*
Control
VGLUT+
E
Failure Rate
1
0.8
0.6
0.4
0.2
0
X
2.5
2
1.5
1
0.5
0
Ca / Mg Ratio
F
Average Failure Rate
1
0.8
0.6
0.4
0.2
0
*
**
Control
VGLUT+

concentration that we found to be optimal for partial attenuation of typical transmission (Figure 5B). A comparison of average traces from before and after antagonist application (Figure 5C) at both Control synapses (left traces) and VGLUT-enhanced synapses (right traces) depicts sample attenuation of Control and VGLUT-enhanced transmission. As shown, the efficacy of γ-DGG in EPSC attenuation was weaker at synapses containing higher levels of VGLUT1. On the whole, γ-DGG reduced the size of control EPSCs by 51%, in contrast to 31% in VGLUT-transfected pairs (Figure 5D, "Control" vs. "VGLUT+" bars; 51 ± 5% vs. 31 ± 11%, respectively; $P < 0.05$ unpaired t-test; $n = 10$ pairs Control; 6 pairs VGLUT+). This line of experiments provides direct evidence that the VGLUT-enhanced synaptic transmission that we observed is indeed due to enhanced presynaptic glutamate release from synaptic terminals.

The amount of glutamate released by synaptic terminals can be varied by changes to the amount of glutamate released per vesicle, which is likely since VGLUT1 can impact vesicle loading (Figure 1). However, we cannot rule out the possibility that VGLUT1 overexpression is instead altering the terminals' probability of release which in turn could impact the likelihood of multiple vesicles fusing simultaneously at the same terminal (multivesicular release) (Tong and Jahr, 1994; Oertner et al., 2002). To directly distinguish between these two possibilities we repeated the above γ-DGG attenuation experiments in a "low probability of release" condition, in which divalent cation concentrations were systematically varied until the observed transmission being evoked not only approximated the quantal size (Figure 4D) but also exhibited a high failure rate. If a low proportion of stimuli results in the release of vesicles, then the proportion of stimuli that foster multivesicular release will be exceedingly low. If vesicles release independently of one another as is widely assumed, and synaptic boutons could be comprised of ~ 10 vesicles (Schikorski and Stevens, 1997), then the probability of a given EPSC involving two or more vesicles can be determined using binomial statistics (see Methods), and MVR will be minimized when probability of release is low, and failure rates are high. Evoked synaptic transmission in Control and VGLUT+ pairs was thus tuned for a high level of baseline failures in each individual pair using different ratios of calcium and magnesium concentrations, as depicted in Figure 5E. As shown in Figure 5F, the average failure rate of transmission used in these experiments was 0.64 for Control pairs and 0.79 for VGLUT+ pairs. Therefore, during transmission in these experiments an upper bound for the incidence of MVR (assuming synapses with ten sites) was ~7% and 3%, respectively, and the majority of synaptic

transmission should have been mediated by single vesicle release events. If the synapses in our study had even fewer release sites, then the likelihood of MVR would have been still further reduced.

Once such a "Low Pr" condition had been achieved in each connection, we measured γ-DGG attenuation. In this new condition favoring the release of single vesicles, γ-DGG attenuation in Control versus VGLUT+ pairs were again significantly disparate (Figure 5D, "Control, Low Pr" vs. "VGLUT+, Low Pr" bars; 52 ± 7% vs. 29 ± 14%, respectively; $P < 0.05$ unpaired t-test; $n = 5$ pairs Control; 5 pairs VGLUT+). Notably, even when the failure rates were made to differ dramatically between "Control" and "Control, Low Pr" (0.41 ± 0.12 vs. 0.64 ± 0.05; $P < 0.05$ unpaired t-test; Figure 5F, left bars) and between "VGLUT+" and "VGLUT+, low Pr" (0.30 ± 0.10 vs. 0.79 ± 0.05; $P < 0.01$ unpaired t-test; Figure 5F, right bars), similar degrees of γ-DGG attenuation were observed irrespective of these manipulations to failure rate. Thus, VGLUT1 overexpression impacts the amount of glutamate released from single vesicles.

VGLUT1 Expression is Developmentally Regulated

While the above results demonstrate the potential of VGLUT1 regulation to alter synaptic transmission and establish the molecule as a limiting step for controlling glutamate release, we were interested in ascertaining whether this control point was utilized endogenously as a physiological mechanism for regulating synaptic transmission. In particular, our previous work (Renger et al., 2001) indicates that developing synapses exhibit several presynaptic functional differences from mature ones, including a reduced number of docking vesicles and less active vesicle cycling, that are rectified during maturation. Given that VGLUT1 can influence transmitter release (Figure 5), we were interested in determining whether an additional maturational change might involve a developmental increase of VGLUT1 expression.

In order to monitor the developmental regulation of VGLUT1, quantitative immunohistochemistry was used to determine the amount of transporter expressed at each stage of development (Figure 6). Immunostaining in mature hippocampal cultures (>DIV14) depicts the transporter as discrete puncta that are tightly co-localized with synaptotagmin (Figure 6A). Repeating this procedure across various stages of development reveals that expression of the transporter appears to markedly increase at

Figure 6. VGLUT1 Expression is Developmentally Regulated and Coincides with a Developmental Change in Quantal Amplitude

(A) Immunolabeling of VGLUT1 and the synaptic marker synaptotagmin Ia across development.

(B) Average proportion, at various developmental stages, of synaptotagmin-labeled puncta that exhibit detectable levels of VGLUT1 protein. Average proportion of VGLUT synapses increases significantly from DIV 6 to DIV 9 (***, $P < 0.001$, unpaired t-test) and from DIV 9 to DIV 20 (**, $P < 0.01$).

(C) Average integrated optical density (IOD) for synapses already expressing detectable levels of VGLUT1. The ratio of VGLUT1 IOD to synapsin I IOD per synapse increases significantly across development from DIV 6 to DIV 9 (**, $P < 0.01$ unpaired t-test) and from DIV 9 to DIV 20.

(D) Miniature excitatory currents (mEPSCs) recorded at different stages of development. Scale Bars: 15 pA, 150 ms. Bottom traces represent an average of a population of events acquired from a single cell at each developmental stage. Scale Bars: 5 pA, 25 ms.

(E) Mean mEPSC amplitude ($n = 8, 8, 6$ cells at DIV 8, 10, 15) increases significantly during development (*, $P < 0.05$ unpaired t-test).

(F) Mean mEPSC frequency also increases significantly between DIV 10 and DIV 15 (*, $P < 0.05$).

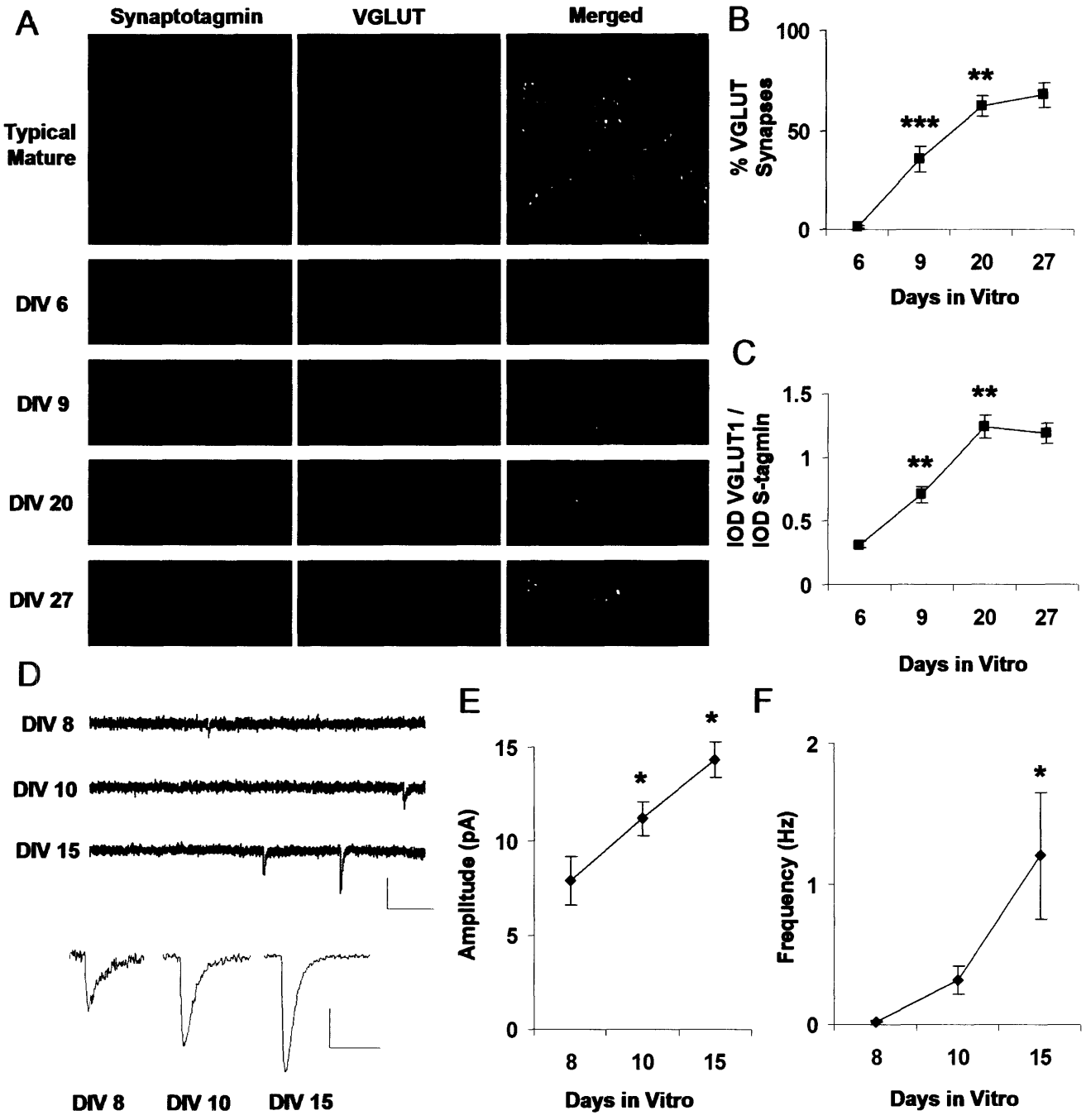
A
Synaptotagmin
VGLUT
Merged
Typical Mature
DIV 6
DIV 9
DIV 20
DIV 27
B
% VGLUT Synapses
100
50
0
***
**
6
9
20
27
Days in Vitro
C
IOD VGLUT1 / IOD S-tagmin
1.5
1
0.5
0
**
**
6
9
20
27
Days in Vitro
D
DIV 8
DIV 10
DIV 15
DIV 8
DIV 10
DIV 15
E
Amplitude (pA)
15
10
5
0
*
*
8
10
15
Days in Vitro
F
Frequency (Hz)
2
1
0
*
8
10
15
Days in Vitro

later stages compared to earlier ones. This maturation results in an increased proportion of synapses expressing detectable levels of VGLUT1 (Figure 6B; $n = 11$ images for each group; DIV 6 vs. 9: $P < 0.001$ unpaired t-test, DIV 9 vs. 20: $P < 0.01$; no significant change between DIV 20 and 27). Of the synapses expressing detectable levels of the transporter, the ratio of VGLUT1 and synaptotagmin integrated optical densities per synapse also exhibits a graded increase across development (Figure 6C; DIV 6 vs. 9: $P < 0.01$ unpaired t-test, DIV 9 vs. 20: $P < 0.01$; no significant change between DIV 20 and 27), indicating that the amount of VGLUT1 protein expressed per synaptic terminal is developmentally up-regulated.

Given that VGLUT1 is up-regulated within synapses across development, we were interested in identifying functional changes that could potentially be related to its gradual expression. One of our observations is that the peak amplitude of quantal excitatory synaptic currents seemed to undergo a strengthening as synapses matured during development (Figure 6D), a trend that was significant across all populations of recorded neurons. mEPSC mean amplitude increased from 7.9 ± 1.3 pA at DIV 8, to 11.1 ± 0.9 pA at DIV 10, to 14.3 ± 0.9 pA by DIV 15 (Figure 6E, $n = 8, 8, 6$ cells respectively, $P < 0.05$ unpaired t-test), thus mirroring a developmental increase that has been reported in brainstem for AMPA receptor-mediated mEPSCs (Ishikawa et al., 2002). While this effect could also coincide with changes in the number and conductance properties of postsynaptic receptors, the significant increase of VGLUT1 protein expressed in synaptic terminals during this period (Figure 6C) could also contribute at least in part to this observed maturational change. Though a significant developmental increase was observed for mEPSC frequency between DIV 10 and DIV 15 (0.20 ± 0.004 Hz, DIV 8; 0.31 ± 0.10 Hz, DIV 10; 1.20 ± 0.45 Hz DIV 15; $P < 0.05$ unpaired t-test; Figure 6F), given our findings on the lack of influence of VGLUT1 expression on mEPSC frequency (Figure 4E) we cannot necessarily conclude that VGLUT1 participates in this phenomenon.

VGLUT1 Expression is Coordinated with the Onset of Functional Vesicle Cycling

Previous work in our group (Renger et al., 2001) has shown that silent synapses can arise in part from incomplete activation of postsynaptic AMPA receptors by a diminished presynaptic release of glutamate. The work demonstrated that conversion from silent to functional transmission could correspond to the developmentally-

regulated onset of "functional" vesicle cycling and the uptake of the FM1-43 styryl dye (Betz and Bewick, 1992). There is thus a developmental delay in FM uptake at early stages of development, and now a delay in VGLUT1 expression as well (Figure 6). We therefore asked whether the delays were coordinated: whether the developmental time course of VGLUT1 expression might be synchronized with the maturation of vesicle cycling. It seemed sensible that as vesicle cycling matures, the functional capacity of transmitter loading needs to be up-regulated accordingly to prevent the release of synaptic vesicles with insignificant transmitter content.

To examine whether such features of presynaptic maturation might be coordinated, it was necessary to concurrently compare the functional capacity of presynaptic terminals with their structural protein content. We made use of AM1-43, a fixable version of FM1-43, to label the functional presynaptic terminals, and followed up with an immunostaining procedure to check the level of desired presynaptic proteins (Renger et al., 2001). It has been shown that the amount FM dye taken up during stimulation can provide an index of the functional capacity of presynaptic terminals. The ability to visualize a fixable version together with immunolabeled protein allowed us to simultaneously measure both VGLUT1 expression levels across development and the developmental onset of functional vesicle cycling. As shown by imaging VGLUT1, AM1-43, and the synaptic vesicle protein synapsin I (Syn I) at the same synaptic terminals (Figure 7A), AM1-43 uptake begins appearing at a similar stage of development as VGLUT1 expression. Figure 7B-D quantifies these developmental changes in a population of synapses, again using integrated optical density (IOD) as a measure of protein expression. Despite a relatively constant level of synapsin I staining across development (Figure 7B), VGLUT1 expression (Figure 7C) appeared to increase in tandem with the onset of AM1-43 labeled functional vesicle cycling (Figure 7D). In general, the ratio of VGLUT1 / Syn I increases from DIV 8 to DIV 15 ($P < 0.001$ unpaired t-test) and from DIV 10 to DIV 15 ($P < 0.001$) in parallel with the ratio of AM1-43 / Syn I ($P < 0.01$, $P < 0.05$) measured at the same synapses (Figure 7E). We thus conclude that the maturation of transporter expression and delivery is jointly coordinated with functional vesicle cycling, a coupling that could be designed to help guarantee the efficient loading of transmitter as vesicle cycling becomes more active.

Figure 7. VGLUT1 Expression is Coordinated with the Onset of Functional Vesicle Cycling

(A) Triple immunostaining for VGLUT1, the functional bouton marker AM1-43, and the vesicle protein synapsin I.

(B) Integrated optical density (IOD) per synapse for synapsin I, an additional vesicle protein, remains relatively stable through development.

(C, D) Synaptic IOD for VGLUT1 and AM1-43 appear to undergo a developmental change.

(E) Mean synaptic integrated optical density per image. Comparing VGLUT1 and AM1-43 intensity levels (with each normalized to synapsin I levels in the same synapse) demonstrates a significant and coordinated increase in VGLUT1 and AM1-43 staining across development. (***, $P < 0.001$, **, $P < 0.01$, *, $P < 0.05$, respectively, unpaired t-tests).

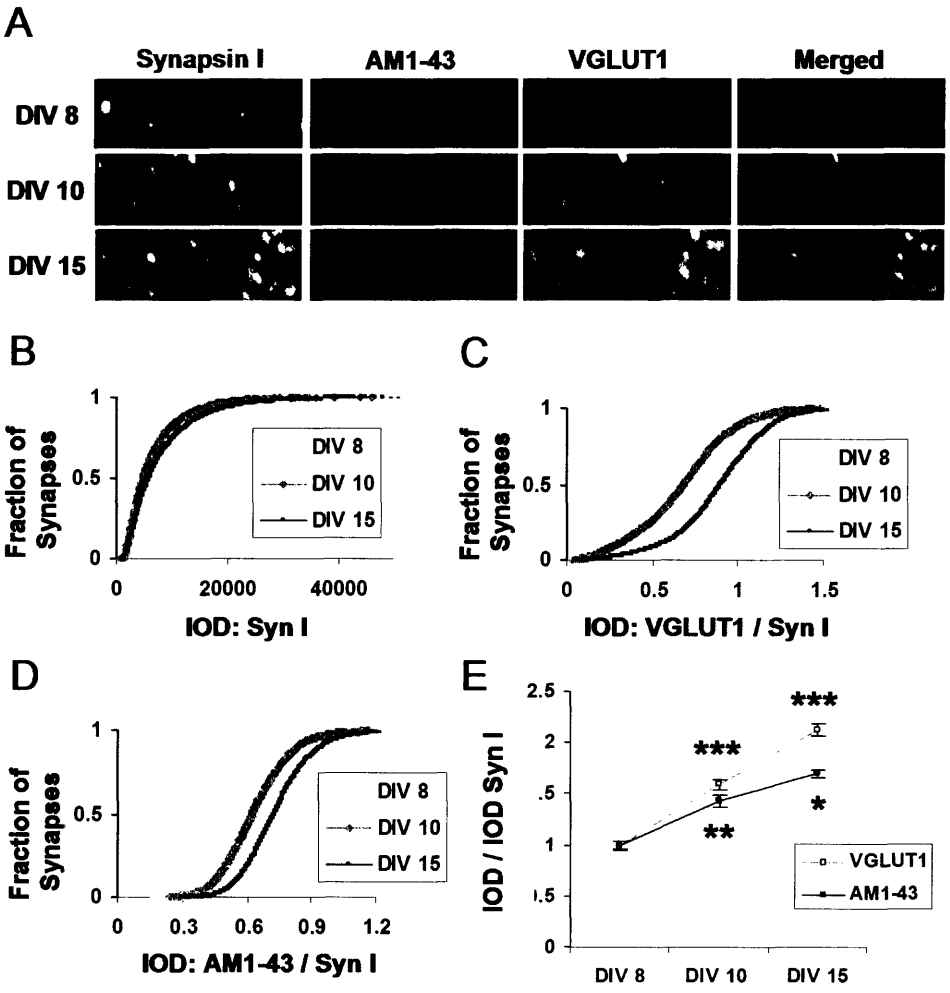
A
Synapsin I
AM1-43
VGLUT1
Merged
DIV 8
DIV 10
DIV 15
B
Fraction of Synapses
1
0.5
0
0
20000
40000
IOD: Syn I
DIV 8
DIV 10
DIV 15
C
Fraction of Synapses
1
0.5
0
0
0.5
1
1.5
IOD: VGLUT1 / Syn I
DIV 8
DIV 10
DIV 15
D
Fraction of Synapses
1
0.5
0
0
0.3
0.6
0.9
1.2
IOD: AM1-43 / Syn I
DIV 8
DIV 10
DIV 15
E
IOD / IOD Syn I
2.5
2
1.5
1
0
***
***
**
*
VGLUT1
AM1-43
DIV 8
DIV 10
DIV 15

Activity Dependent Plasticity of Glutamate Release and VGLUT1 Expression in Mature Circuits

Exciting work by others (Turrigiano et al., 1998; Burrone et al., 2002; Thiagarajan et al., 2002) has recently demonstrated that excitatory synapses undergo activity-dependent plasticity in quantal size in response to global changes in network activity. Mechanisms have been proposed to begin to explain this change in quantal size, including changes in postsynaptic receptor number (O'Brien et al., 1998; Watt et al., 2000; Wierenga et al., 2005). Given that molecules responsible for specifying the quantal size postsynaptically, such as AMPA receptors, appear to be critically regulated during activity-dependent synaptic scaling, we decided to examine whether VGLUT1 expression might provide a complementary presynaptic mechanism by which quantal size can be coordinately regulated via endogenous, homeostatic control.

We therefore measured VGLUT1 expression levels per synaptic terminal by again taking the integrated optical density (IOD) ratio of VGLUT1 to synapsin I at each immunolabeled synapse as before, but now comparing between untreated control cultures vs. cultures that were pre-incubated for 48 hours in 20 μM bicuculline, for the purpose of chronically increasing activity levels by blocking $GABA_A$ receptor-mediated inhibitory currents (Turrigiano et al., 1998) (Figure 8A). We observed that chronic increases in activity levels (BIC) led to a significant reduction in synaptic VGLUT1 expression relative to control values (0.75 ± 0.06 Control vs. 0.95 ± 0.03 BIC; $P = 0.02$ unpaired t-test; $n = 8$ images, 4482 synapses Control; 7 images, 4464 synapses BIC; Figures 8B). We then attempted the exact opposite condition, chronically blocking AMPA and NMDA-type excitatory receptors by applying either 5 μM NBQX or 50 μM AP5 to effectively decrease activity levels through each one of these pathways (Thiagarajan et al., 2002; Liu, 2004) and measuring the resulting expression levels of VGLUT1. Here, while we observed a robust increase in VGLUT1 in response to chronic NMDA receptor blockade (Figures 8A and 8B), a less prominent increase and a surprising variability were disclosed in response to AMPA receptor blockade (Supplementary Data) – this dichotomy were confirmed by replicating the experiments for NBQX and AP5 many times. NMDA receptor blockade, however, resulted in increased VGLUT1 expression across every instance tested, and in the experiment presented in Figures 8A and 8B increased VGLUT1 / Syn I levels by $35 \pm 4\%$ relative

Figure 8. Activity-Dependent Plasticity of VGLUT1 Expression and Glutamate Release
(A) Double immunostaining for VGLUT1 and the vesicle protein synapsin I following 48 hr. incubation with either bicuculline (BIC) to block $GABA_A$ receptors and increase neuronal activity, or AP5 to block NMDA receptors and decrease neuronal calcium flux.
(B) Mean VGLUT1 expression (VGLUT1 IOD normalized by synapsin I IOD at the same synapse) was reduced following chronic $GABA_A$ receptor blockade (*, $P = 0.02$ unpaired t-test, values scaled to Control) and enhanced by chronic NMDA receptor blockade (***, $P < 0.001$ unpaired t-test, values scaled to Control).
(C) Comparison of EPSC amplitude attenuation by 600 μM γ-DGG in Control, BIC and AP5-treated cultures. Each data point represents an average of 3 adjacent sampled EPSCs (0.2 Hz). Shown are representative pre- and post-DGG baselines, normalized to their respective pre-drug levels for comparison.
(D) Typical attenuation of Control, BIC and AP5-treated EPSCs by 600 μM γ-DGG in the paired connection exhibiting median attenuation for the group. Traces are EPSCs averaged from multiple samples of a single connection, normalized by pre-drug amplitudes for direct comparison.
(E) Summary data of γ-DGG attenuation across multiple connections: BIC-treated transmission is significantly more attenuated than non-treated control transmission (*, $P < 0.05$ unpaired t-test, values scaled to Control). AP5-treated transmission is significantly less attenuated than non-treated control transmission ($P < 0.01$, unpaired t-test, values scaled to Control).
(F) γ-DGG attenuation measured in mEPSCs as an additional control. BIC-treated transmission is significantly more attenuated by γ-DGG application than non-treated control mEPSCs (*, $P < 0.05$ unpaired t-test), indicating that observed changes in glutamate release correspond to differences in per vesicle glutamate release.
(G) Sample mEPSCs from bicuculline-treated (BIC), Control, or AP5-treated cultures (Scale bars: 15 pA, 150 ms).
(H) Mean mEPSC amplitude is significantly reduced in BIC-treated cultures compared to non-treated control cultures, and is significantly elevated in AP5-treated cultures (*, $P < 0.05$ unpaired t-test).

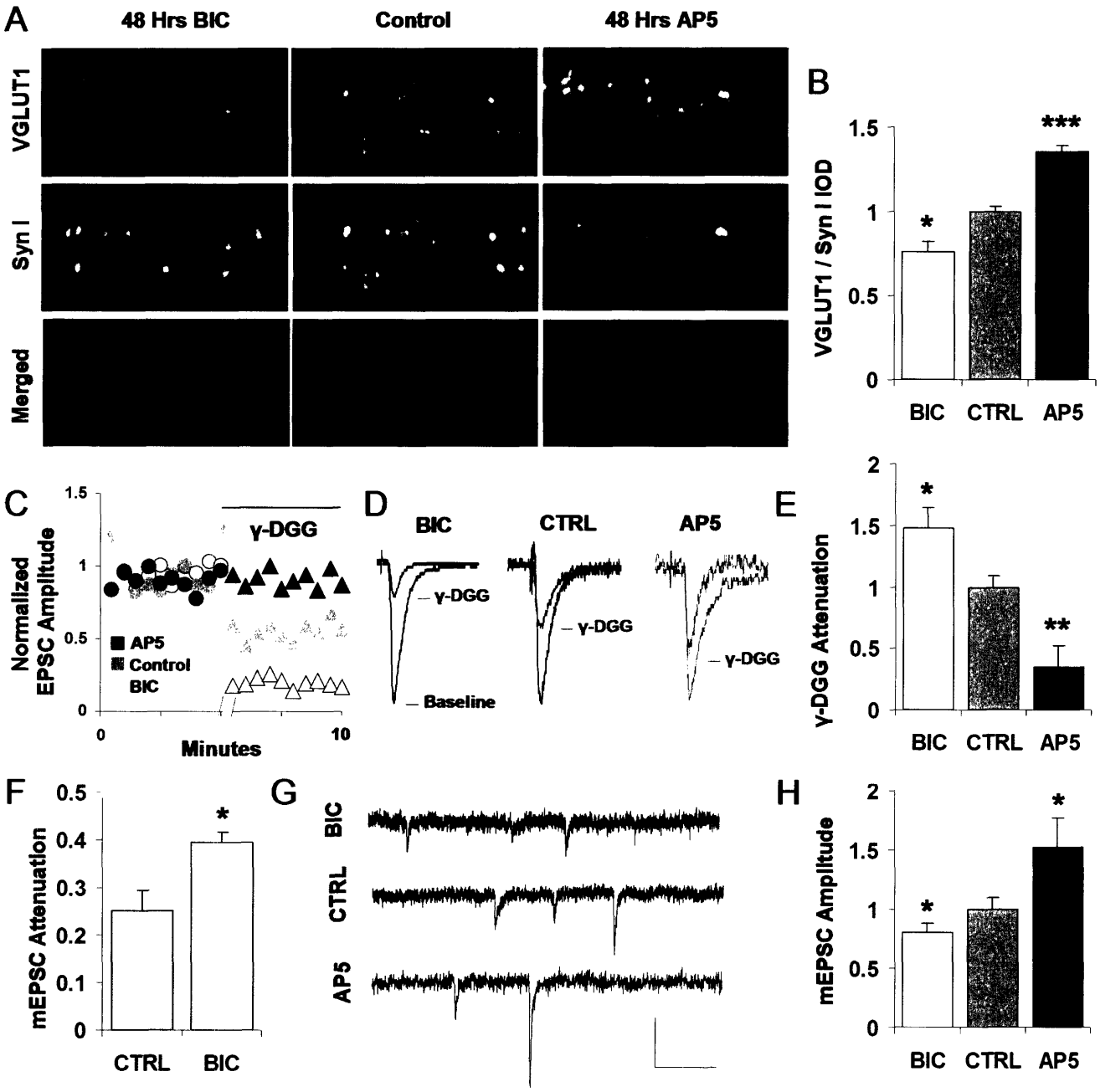
A
48 Hrs BIC
Control
48 Hrs AP5
VGLUT1
Syn I
Merged
B
VGLUT1 / Syn I IOD
1.5
1
0.5
0
*
***
BIC
CTRL
AP5
C
Normalized EPSC Amplitude
1.5
1
0.5
0
γ-DGG
AP5
Control
BIC
0
10
Minutes
D
BIC
CTRL
AP5
γ-DGG
γ-DGG
γ-DGG
Baseline
E
γ-DGG Attenuation
2
1.5
1
0.5
0
*
**
BIC
CTRL
AP5
F
mEPSC Attenuation
0.5
0.4
0.3
0.2
0.1
0
*
CTRL
BIC
G
BIC
CTRL
AP5
H
mEPSC Amplitude
2
1.5
1
0.5
0
*
*
BIC
CTRL
AP5

to Controls ($P < 0.001$ unpaired t-test; $n = 10$ images, 6120 synapses Control; 8 images, 6532 synapses AP5).

Thus, VGLUT1 expression appears to be capable of bi-directional endogenous regulation in response to changes in activity patterns, which could provide a mechanism for presynaptic terminals to coordinate functionally with activity-dependent changes to their postsynaptic partners. To verify that such changes to expression levels indeed had functional implications, we next measured whether glutamate release was also changing as a result of the activity-dependent VGLUT1 regulation. In order to examine activity-driven changes in glutamate release, we repeated our competitive antagonism protocol applied earlier (Figure 5), again in mature hippocampal cultures, except that in this case one set of cultures was pre-incubated for 48 hours in either 20 μM bicuculline (BIC) or 50 μM AP5. In these experiments the cleft glutamate concentration at non-treated synapses appeared to be similar to that observed earlier (Figure 5D), with an approximate 50% reduction in evoked postsynaptic current in response to 600 μM of γ-DGG (Figures 8C, gray symbols, and Figure 8D, middle traces). Bicuculline-treated synapses, however, were significantly more sensitive to the antagonist (Figures 8C, white symbols, and Figure 8D, left traces), and led to 47% more attenuation than Control (76 ± 4% vs. 51 ± 3%; $P = 0.03$ unpaired t-test; $n = 4$ pairs BIC; 4 pairs Control; Figure 8E), indicating that the bicuculline-treated terminals released less glutamate, thus rendering their transmission more susceptible to the effects of the antagonist. To examine whether a comparable change in glutamate release was also observed in the opposite direction following a treatment that up-regulates VGLUT1, we repeated this comparison with chronically-treated AP5 cultures. Here we observed that the antagonist was significantly less effective on AP5 treated transmission (Figure 8C, black symbols, and Figure 8D, right traces), whereby the γ-DGG block was reduced by 65% in AP5 synapses compared to Control transmission (20 ± 8% AP5 vs. 61 ± 5% Control; $P < 0.01$ unpaired t-test; $n = 6$ pairs AP5, 6 pairs Control; Figure 8E).

Since the activity-dependent changes that altered vesicular glutamate release (Figures 8C-8E) also impacted VGLUT1 expression (Figures 8A and 8B), and since our earlier data demonstrates a causal relationship between VGLUT1 expression and glutamate release, we interpret our observed changes in glutamate release under BIC and AP5 treatments to occur largely as a direct consequence of the altered VGLUT1 expression. However, if synaptic terminals can at times undergo multivesicular release (MVR) from single release sites, then the cleft glutamate concentration could also be

altered in part by changes to the number of vesicles released from single terminals. This is possible given evidence that the probability of release, and thus the prevalence of MVR-mediated changes to cleft glutamate concentration, can be modified by perturbations to network activity levels (Murthy et al., 2001). As an additional control to further verify that these changes correspond to changes to the loading of single vesicles, we also measured the cleft glutamate concentration during spontaneous, miniature EPSCs in the bicuculline-treated transmission (Figure 8F). Here we observed that median γ-DGG attenuation was significantly increased relative to controls (Figure 8F; 25 ± 4 % Control vs. 39 ± 2 % BIC, $P = 0.02$, unpaired t-test), although the attenuations observed in the mEPSCs were less than those in the EPSCs, presumably due to the detection problems associated with spontaneous transmission when it is pharmacologically reduced (Zhou et al., 2000) which likely serves to underestimate the attenuation in the control condition, and to a greater degree the smaller amplitude bicuculline-treated condition. Even with this detection problem, significant changes in the amount of glutamate released from single vesicles were observed between the two treatments.

To verify that activity-induced changes to VGLUT1 expression were also accompanied by changes to quantal synaptic efficacy, we quantified the amplitude of spontaneous mEPSCs. Here we observed that in bicuculline-treated transmission, mEPSC amplitude was significantly reduced compared to control transmission (Figure 8G, top trace and Figure 8H, $n = 6$ Control; $n = 4$ BIC; $P = 0.04$, unpaired t-test), while in AP5-treated transmission, mEPSC amplitude was increased by 52% from control transmission (Figure 8G, bottom trace and Figure 8H, $n = 7$ Control; $n = 6$ AP5; $P = 0.03$, unpaired t-test). Thus in both cases activity-induced changes to VGLUT1 expression are accompanied by changes to quantal synaptic efficacy.

As such, chronic changes to either levels of activity or calcium flux alter vesicular transporter expression in a manner that is accompanied by relevant changes to physiological transmission. Endogenous control over VGLUT1 provides one mechanism by which an observed presynaptic scaling of glutamate release could be coordinated with a concomitant scaling of postsynaptic sensitivity (Watt et al., 2000).

DISCUSSION

For neurons to be able to make use of VGLUT1 expression to modulate transmission makes specific predictions on a set of issues that remain controversial at glutamatergic synapses. By following the impact of transporter number through vesicle loading (Figure 1), glutamate release (Figure 5), and postsynaptic receptor activation (Figures 3 and 4), we provide new evidence in support of a flexibility in excitatory vesicle filling (Atwood and Karunanithi, 2002) and a non-saturation of hippocampal synapses (Auger and Marty, 2000; Liu, 2003). Further, while it remains undemonstrated whether presynaptic mechanisms endogenously contribute to regulating the quantal efficacy of excitatory transmission, we show that VGLUT1 expression can confer some properties of this regulation to excitatory synapses.

Vesicle Loading Depends on the Number of Available VGLUT1 Transporters

It is imaginable that vesicles set in a low concentration of glutamate might simply continue filling until they have reached a "set point" level of saturation (Sulzer and Pothos, 2000), such that adding transporters could influence the speed, but not the final concentration, of glutamate uptake. The work presented here indicates that VGLUT1 vesicles do not fill to an invariant set point, and that reducing the pool of participating transporters (Figures 1) reduces the equilibrium value of uptake, though it still cannot be resolved whether this is accomplished by changing the intravesicular concentration of transmitter, or instead the structural capacity of the vesicle (Bruns et al., 2000; Colliver et al., 2000; Sulzer and Edwards, 2000; Karunanithi et al., 2002).

VGLUT1 Overexpression Enhances Excitatory Synaptic Transmission, via an Increase in Glutamate Released Per Vesicle

We then found that it was possible to traffic additional functional VGLUT1 protein to synaptic terminals (Figure 2), where we consequently observed larger evoked and spontaneous excitatory currents (Figures 3 and 4) as a result of an increased cleft glutamate concentration (Figure 5). We provide direct verification that vesicular transport is able to exploit receptor non-saturation at the level of single vesicles via a shift in the cleft glutamate concentration. An additional finding of some surprise was that VGLUT1 overexpression resulted in a decrease in evoked failure rate (Figure 3E). This could suggest that in addition to enhancing the amount of glutamate deposited per

release event, VGLUT1 expression might also be able to influence the likelihood that such release events will occur. Interestingly, another recent study reports that loss of VGLUT1 expression results in a substantially depleted pool of synaptic vesicles at excitatory terminals (Fremeau et al., 2004). Such a relationship between VGLUT1 expression and likelihood of release could depend on either the presence of the transporter itself, or on the extent of filling that it facilitates.

It is also important to consider whether VGLUT1 expression could contribute to synaptic efficacy by influencing not only the *amount* of filling but also the *rate* (Sulzer and Pothos, 2000). This is especially plausible given two recent studies into the nature of vesicle cycling (Aravanis et al., 2003; Gandhi and Stevens, 2003), which confirmed a "kiss-and-run" type of release that involves the brief fusion and rapid re-use of synaptic vesicles. Such efficiency in cycling would place high demands on vesicle filling to prevent the "firing of blanks" via the exocytosis of "empty" vesicles. While the precise speed of vesicle filling in the endogenous context can only be estimated, loading in vesicles isolated from brain (Figure 1) and (Maycox et al., 1988; Wolosker et al., 1996) as well as loading in BON and PC12 cell lines (Bellocchio et al., 2000; Takamori et al., 2000), have been shown to involve a relatively slow process (several minutes), compared to the rapid process of vesicle re-use (~20 s) (Aravanis et al., 2003). A rapid turn-over of vesicles could thus result in a depleted synaptic response, and an increasing degree of transporter expression may be important for ensuring a match between the speed of transmitter loading and the functional capacity of the release machinery. Indeed, VGLUT1 is up-regulated in close register with the increase of vesicle cycling that occurs during synaptic maturation (Figure 7), and down-regulated during activity-dependent scaling (Figure 8) in parallel with a reduction in probability of vesicle release (Murthy et al., 2001).

Vesicular Transporter Expression is Endogenously Regulated

We found that transporter levels are modified endogenously across development (Figure 6) and by levels of activity (Figure 8). If vesicular transporters do contribute meaningfully to synaptic transmission, it would not be surprising to find them amidst a molecular ensemble of similar versatility to that in the postsynaptic density (Sheng and Kim, 2002). Molecular studies at inhibitory synapses, for example, have recently uncovered a direct association between the vesicular GABA transporter VGAT and the

synthetic enzyme GAD65 (Jin et al., 2003), suggesting that transmitter synthesis may be functionally coupled to vesicle loading. The fact that VGLUT1 expression is coordinated with the onset of functional vesicle cycling (Figure 7) could in turn suggest a conjunctive signal that couples fusion with adequate filling, to ensure that increasingly active vesicles are able to release meaningful quantities of transmitter, perhaps in coordination with a growing pool of receptors postsynaptically.

Similarly, a negative-feedback relationship between certain forms of synaptic activity and VGLUT1 expression which adjusts glutamate release in response to either circuit excitability or calcium influx (Figure 8) could provide a presynaptic means for maintaining a stable degree of activity in the face of changing input levels (Turrigiano and Nelson, 2000) in a manner congruent with other recently uncovered postsynaptic mechanisms (O'Brien et al., 1998; Watt et al., 2000; Thiagarajan et al., 2002). Chronic blockade or enhancement of synaptic activity has previously been shown to lead to compensatory shifts in the size of the readily-releasable pool and the number of presynaptic active zones (Murthy et al., 2001). This observation has supported a "size principle" (Harris and Stevens, 1989; Pierce and Lewin, 1994; Schikorski and Stevens, 1997) in which functional changes in morphology can correspond to changes in the size of the presynaptic terminal or postsynaptic density (PSD). It is possible that an activity-driven scaling of presynaptic terminal size (Murthy et al., 2001) is similarly accompanied by alterations in transporter expression per vesicle (Figure 8), to provide a presynaptic shift in quantal efficacy that coincides with the known activity-driven changes in probability of release. On the other hand, while blocking inhibitory receptors was effective at scaling VGLUT1, we were surprised to find that blocking NMDA receptors triggered a more profound regulation than observed while blocking AMPA receptors. This suggests that VGLUT1 regulation, at least in hippocampal synapses, may be more sensitive to calcium flux than postsynaptic membrane depolarization, though other regimes of regulation may be more prominent in cortical synapses (Watt et al., 2000; Pratt et al., 2003) depending on the layer of cortex and which vesicular transporter is expressed.

Most likely, further work will elucidate a range of distinct modes by which vesicular transport contributes to the dynamics of synaptic efficacy, as well as distinct isoforms by which those contributions are made. Independent regulation of VGLUT1 and its recently identified isoforms VGLUT2 (Fremeau et al., 2001; Takamori et al., 2001; Varoqui et al., 2002) and VGLUT3 (Fremeau et al., 2002; Schafer et al., 2002),

could in particular offer exciting clinical possibilities. Already, the first mutations to the VGLUT1 ortholog *eat-4* in Xenopus have revealed the importance of vesicular transport in both short-term (Rankin and Wicks, 1995) and long-term (Rose et al., 2002) memory. Future studies into the regulation of transmitter loading and release should thus discern new principles by which adaptations on both sides of the synapse are coordinated to ensure a cohesive robustness of memory.

SUPPLEMENTARY DATA

A. Changes Observed across all VGLUT Regulation Experiments:

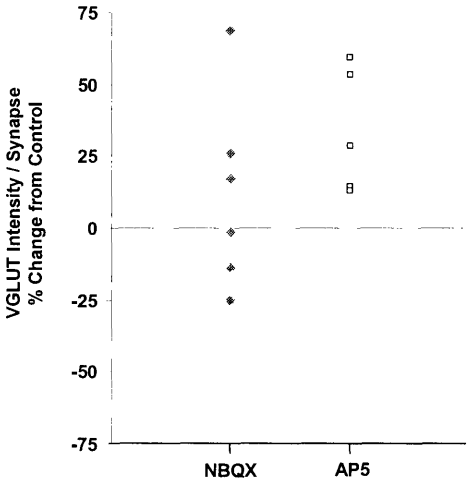

A. Regulation of VGLUT1 expression by chronic blockade of AMPA receptors (NBQX) or NMDA receptors (AP5). Each dot represents one set of experiments depicted in Figure 8B. NBQX treatment was observed to up-regulate VGLUT1 by as much as 68%, lead to no change at other times, and even down-regulate it by as much as 25%. AP5 treatment in contrast had a reduced variability in its effects, and resulted in up-regulation of VGLUT1 during all experiments.

B. Summary of all immunostaining VGLUT Regulation Experiments:

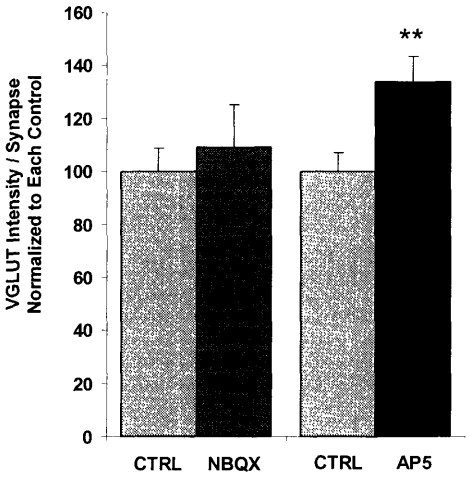

B. Summary data of (A). NBQX treatment resulted in more variable VGLUT1 regulation for a lower average increase compared to AP5 treatment (**, $P < 0.01$).

CHAPTER 2

Scaling of Synaptic Efficacy as a Function of Number of Available Synaptic Partners

PROLOGUE

The control of neuronal positioning and outgrowth is of fundamental importance to a range of potential technologies ranging from cellular biosensors to tissue engineering, but may also find important applications as a vital tool for the highly controlled study of neuronal interactions. With this in mind, the following body of work emerged serendipitously from an attempt to overcome a technical challenge. During my first year, my research advisor had pointed out that the ability to pattern the two-dimensional structure of where cultured neurons could grow and not grow was essential for creating separate sub-networks that could then be led to interact in controlled and interesting ways.

After working for several years on a way to accomplish this systematic patterning of neurons, I arrived at a particularly promising method based on soft photolithography. As a test for applying this method to neurons for the first time, we tried to imagine the simplest structural characteristic of a group of neurons that we could think of to vary, and deduced that simply "size of the island", or the number of neurons on it, was one simple property, and set out to craft circuits in which size was systematically varied.

We finally got the new patterning method to work, and one of the first verifications of the methodology was to see whether the micropatterned cultures were biologically active. From the first measurements with the electrode, I quickly realized something interesting– not only were the neurons on every island, large or small, firing action potentials in a healthy manner, but all neurons were doing so at approximately the same rate, no matter how many other neurons were present on the island to drive activity.

We tend to consider neurons as classical input-output devices – integrators which fire to the extent that they are solicited to by their projections. In this case however it seemed that no matter what the amount of input that should have been going into a given neuron from its neighbors, the output amount was always similar. An attempt to elucidate this phenomenon forms the basis for the following section.

INTRODUCTION

In highly plastic regions of the brain such as the hippocampus and cerebral cortex, excitatory synapses are believed to adjust their strength dynamically in order to ensure the effective propagation of information through the network. If network activity levels are low, neurons will scale up the strengths of their synapses to become more sensitive to sparse transmission events. If activity levels are high, neurons will scale down the strengths of their synapses to maintain firing rates within a functional range that is more physiologically meaningful.

We hypothesized that a related "inverse rule" might be invoked to tune the strength of a neuron's inputs as a function of the size of the network in which it is situated. For example, if the aggregate synaptic drive to or from a cell were a "finite resource" that is distributed among each of its synaptic partners, then a large network in which a cell has more synaptic partners would incur weaker inputs than a comparable network of fewer partners.

To directly test this prediction, we made use of photolithographic microstructures to construct cultured neuronal networks of precisely controlled sizes. Microlithographs of different sizes were able to sustain a constant neuron and glial cell density, a stable excitatory / inhibitory neuronal subtype ratio, and stable action potential firing frequencies across differently sized islands, suggesting that micropatterned cultures were biologically stable and functionally active.

However, larger networks that contained more neurons, and involved more synapses exhibited a reduced unitary conductance per excitatory synapse than smaller networks. Furthermore, neurons in larger networks were connected more sparsely and more weakly with individual partners, and underwent a reconfiguration of synaptic identity and targeting to further stabilize activity levels.

These observations indicate that neurons in plastic circuits may endogenously trade off a few strong connections with a small number of neighbors for more numerous, weaker connections when additional neighbors are introduced. In this framework, negative feedback forms of plasticity could provide a fundamental mechanism for network processing, by enabling cells to alter the strengths of their inputs in proportion to the number of synapses and cells in their local microcircuit.

RESULTS

A system for designing the geometry of cultured neuronal networks in order to grow identical networks of varying size.

The earliest work in patterned neuron cultures employed small islands of adhesive protein or cells arranged over an inhibitory background such as agarose gel so that each island contained a small number of neurons. Such cultures simplified studies of synapses between neurons and cardiac myocytes by limiting connections in several of the myocytes islands to a single neuron (Furshpan et al., 1976). Though the technique relied on a relatively simple airbrush procedure to generate the tiny droplets, the sizes and locations of the islands were arbitrary, and only round islands could be produced. Newer, more controlled patterning techniques for biological cells in an increasing number of fields have included contact masks (Westermark, 1978), photolithography using photoresists (Kleinfeld et al., 1988; Wyart et al., 2002) and photochemistry (Hickman et al.,1994), microstamping (Branch et al., 2000; Scholl et al., 2000; Wheeler et al., 1999), and microfluidic channels (Martinoia et al., 1999).

For our methodology for the patterning of cultured neurons, AutoCAD software from Designers' CADD Company, Inc. was used to create a micropattern of increasingly larger squares which was repeated over three rows. The photomask was custom printed by Advance Reproductions Corporation onto a transparency and transferred, via UV exposure and developing, onto silicon wafers which were covered in a thin layer of photoresist (Silicone Sense, Incorporated).

The remainder of the procedure is detailed graphically in Figure 1A. The resulting features of the photoresist were used as a mold to create a microstamp. For this segment in the fabrication process, poly(dimehylsiloxane) (PDMS; Dow Chemical Company) was poured onto the silicone wafer and cured with heat. After cooling, the PDMS was then peeled from the wafer, whereupon it contained the imprint of geometric features of the squares described above.

An electron-beam evaporator at the Whitehead Institute was used to deposit a thin layer of gold and titanium onto the surface of a glass coverslip (titanium: Cat. No. 43367-5; gold: Cat. No. 37316-8; both from Sigma-Aldrich). This coverslip was used as the solid substrate upon which the microstamp was put in contact. That is, the PDMS stamp was "inked" with hydrophobic alkanethiols (purchased and purified before use), dried with nitrogen gas, and brought into tight contact with the surface of the coverslip. Consequently, the hydrophobic alkanethiol molecules were transferred onto the regions

Figure 1. A system for designing the geometry of cultured neuronal networks in order to grow identical networks of varying size.

(A) Schematic of method for generation of micropatterned culture. Features of photoresist carved by ultraviolet light were used as a mold to create a microstamp, formed from poly(dimehylsiloxane) (PDMS) which was poured onto the silicone wafer and cured with heat. After cooling, the PDMS was then peeled from the wafer, whereupon it contained the imprint of geometric features from the desired template. An electron-beam evaporator at the Whitehead Institute was then used to deposit a thin layer of gold and titanium onto the surface of a glass coverslip. This coverslip was used as the solid substrate upon which the microstamp was put in contact. The microstamp was "inked" with hydrophobic alkanethiols (purchased and purified before use), dried with nitrogen gas, and brought into tight contact with the surface of the coverslip. Consequently, the hydrophobic alkanethiol molecules were transferred onto the regions of the glass surface that only contacted the raised regions of the stamp. Once the alkanethiols were transferred to the gold surface, they immediately formed self assembled monolayers limited to the square islands. Just before deposition of primary cell culture of hippocampal neurons, a solution of laminin at 50 μg/ml was used to coat the square islands, as only the hydrophobic surfaces allowed physiosorption of protein. The PEG covered nonadhesive regions remained free of laminin in addition to repelling any extracellular matrix deposition by neurons themselves. When hippocampal neurons were plated onto the laminin coated micropatterned substrates, they preferentially attached to the islands and spread to assume the island's size and shape.

(B) Neurons took root and eventually exhibited morphology similar to that observed in normal dissociated cultures.

(C) Result of micropatterning neurons in a cross-stitch pattern.

(D) Corner of a square microisland of neurons labeled with the excitatory neuron marker α-CaMKII.

(E) Example of how small the islands can be crafted to support neurons. Islands this small were not used in the remaining experiments.

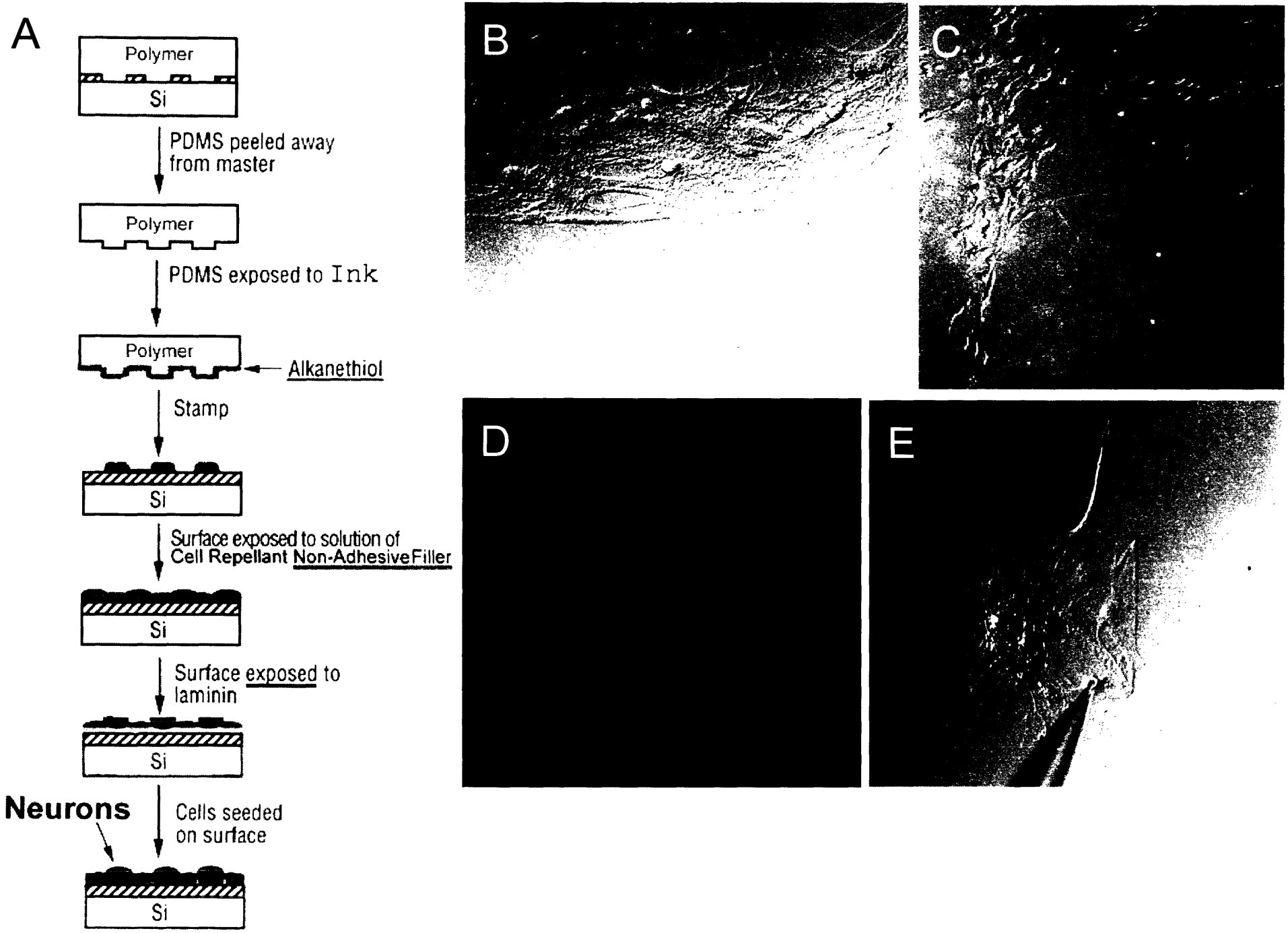
A
Polymer
Si
PDMS peeled away from master
Polymer
PDMS exposed to Ink
Polymer
Alkanethiol
Stamp
Si
Surface exposed to solution of Cell Repellant Non-AdhesiveFiller
Si
Surface exposed to laminin
Si
Neurons
Cells seeded on surface
Si
B
C
D
E

of the glass surface that only contacted the raised regions of the stamp. Once the alkanethiols were transferred to the gold surface, they immediately formed self assembled monolayers limited to the square islands.

Chemicals as well as the synthesis of nonadhesive alkanethiol SAMs were supplied through a developed collaboration with Dr. Michael Ty and laboratories at Harvard Medical School. They included (tridecafluor-1,1,2,2-tetrahydrooctyl)-1-trichlorosilane, tetrahydrofuran, deuterated chloroform, 11-brmoundec-1-ene, calcium hydride, hexadecanethiol, hexanes, sodium hydroxide, benzophenone, dichloromethane, sodium sulfate, recrystallized 2,2'-azobisisobutyronitrile, thiolacetic acid, sodium methoxide, tri(ethylene glycol), and DL-camphor-10-sulfonic acid. Other common basic laboratory equipment and materials (e.g., thin-layer chromatography, column chromatography, nuclear magnetic resonance, 450-W medium-pressure mercury lamp, ace glass, rotary evaporator) were also kindly supplied. The nonadhesive alkanethiolate, (1-mercaptoundec-11-yl)tri(ethylene glycol), was created by first combining (undec-1-en-1-yl)tri(ethyleneglycol) with sodium hydroxide, tri(ethylene glycol), and 11-bromoundec-1-ene. This product was then purified and used to synthesize {1-[(methylcarbonyl)thio] undec-11yl}tri(ethylene glycol), and eventually the final nonadhesive product.

After a few minutes to allow permanent stabilization of the adhesive SAMs, a solution containing the nonadhesive poly(ethylene glycol)-alkanethiolate (PEG), which contains terminal triethylene glycol groups was added. The nonadhesive alkanethiol similarly formed a SAM between the adhesive regions, and a continuous SAM thereby formed over the entire glass surface. Just before deposition of primary cell culture of hippocampal neurons, a solution of laminin at 50 μg/ml was used to coat the square islands, as only the hydrophobic surfaces allowed physiosorption of protein. The PEG covered nonadhesive regions remained free of laminin in addition to repelling any extracellular matrix deposition by neurons themselves. When hippocampal neurons were plated onto the laminin coated micropatterned substrates, they preferentially attached to the islands and spread to assume the island's size and shape. Cells settling outside of patterned regions were either washed off by rinsing the substrates, or died within the first days of culture, often due to a reduced extension of processes that may have been critical for stabilization.

After 14 days of incubation to allow circuits to mature within each network size, the stability of neurons on the substrates was assessed. Neurons took root and

eventually exhibited morphology similar to that observed in normal dissociated cultures (Figure 1B), and adhered with high fidelity to borders defined in the pattern whether the pattern was a cross-stitch (Figure 1C) or square islands (Figure 1B; Figure 1D-1E).

In order to create neuronal islands of systematically varied size, a template was used involving four squares of geometrically increasing diameter (Figure 2). Figure 2A illustrates a gold-based micropatterned chip during experiments, in which the larger squares are visible to the eye. An important feature of these patterns is that a substantial number of neurons were also cultured around the perimeter of the squares, so as to further facilitate the general survival of all neurons on the chip, by contributing trophic and other factors which presumably diffused to be shared somewhat evenly across all islands.

Using confocal microscopy to detect fluorescence at 10x upon labeling with a somatic and dendritic marker such as α-CaMKII, it was possible to clearly delineate the borders of where cells and dendritic networks no longer grew. The sharpness of these borders was assessed and the height and width of squares was then measured using FluoVIEW software spatial calibration tools. Neuronal island diameter, as measured from the borders formed by the tissue itself, was controlled quite rigorously, with only small deviations across cultures (Figure 2B). A reconstructed example of the actual micropatterned cultures used in experiments is depicted in Figure 2C. As shown, the system thus allowed for the systematic specification of network morphology and allowed us to design remote islands of precise sizes to vary the number of neurons comprising a network.

Figure 2. Neuronal islands of systematically varied size.

(A) A gold-based micropatterned chip as seen during experiments, in which some of the larger squares are visible to the eye. An important feature of these patterns is that a substantial number of neurons were also cultured around the perimeter of the squares, so as to further facilitate the general survival of all neurons on the chip.

(B) Using confocal microscopy to detect fluorescence at 10x upon labeling with a somatic and dendritic marker such as α-CaMKII, it was possible to clearly delineate the borders of where cells and dendritic networks no longer grew. Neuronal island diameter, as measured from the borders formed by the tissue itself, was controlled quite rigorously, with only small deviations across cultures.

(C) A reconstructed example from many images of the actual micropatterned cultures used in experiments.

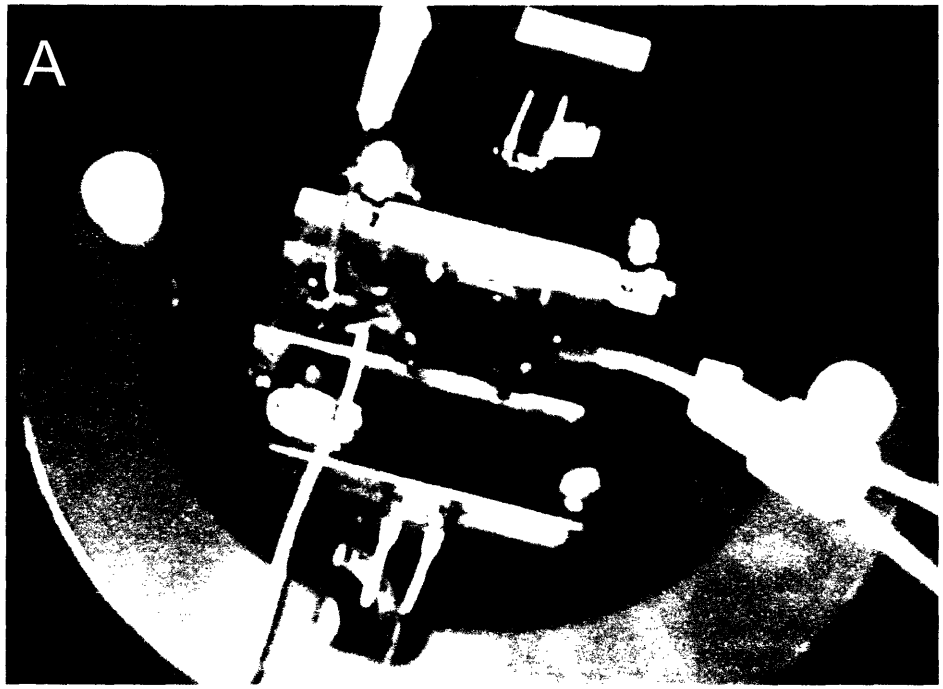
A

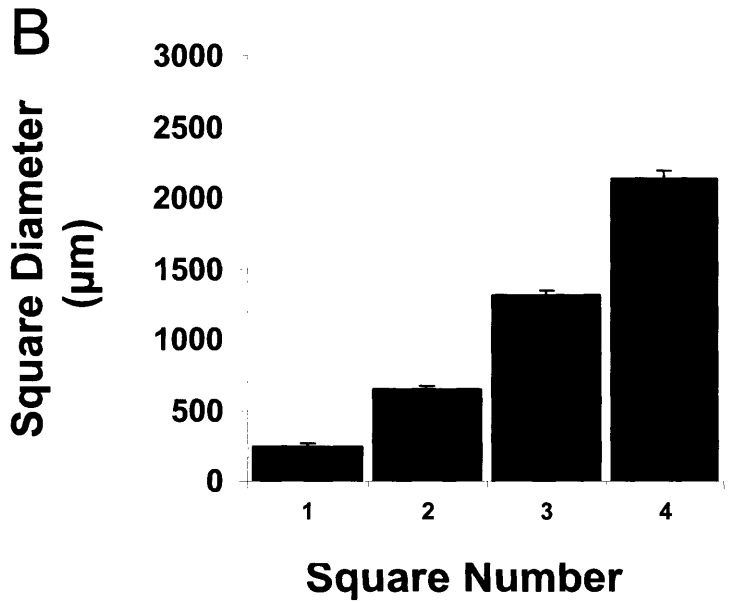
B
Square Diameter (µm)
3000
2500
2000
1500
1000
500
0
1
2
3
4
Square Number


C
1 mm

Neurons on micropatterned islands exhibit robust structural and functional properties

Once networks have developed and neurons have fully extended processes and formed synaptic connections (> DIV 14), the neurons were assessed for vitality to verify normal development and function. Neurons isolated to squares were first identified as DAPI-labeled cell bodies stained for the neuronal marker MAP2 following fixation in paraformaldehyde (Figure 3A). A higher magnification view revealed a heterogeneous mix of DAPI-labeled cells with and without co-expression of MAP2 and the synaptic marker VGLUT1 (Figure 3B). We interpret this to indicate that both neurons and non-neuronal glial support cells were present and that synaptic connections had formed between the neurons. The presence of synaptic connections was further elucidated with the presynaptic marker synapsin I (Figure 3Ci) which appeared as localized puncta along neuronal dendrites. Synapses were verified as functional using the optical marker FM1-43 (Betz and Bewick, 1992) (Figure 3Cii). While the opacity of the gold chips made it impossible to perform the high-quality imaging without fixation that live imaging requires for best results, we could at least visualize non-quantitatively the presence of functional vesicle turnover.

Neurons were also immunolabeling with α-CaMKII and GABA to label the full extent of excitatory and inhibitory cell bodies and dendrites (Figure 3D). Cell bodies can be visualized as bright puncta relative to diffuse dendritic staining, and the occurrences of these somata can be counted manually while panning around the square with the imaging system. This enabled us to compare survival ratios across the different islands and ensure that a similar ratio of excitatory and inhibitory neurons survived to contribute to network dynamics. As shown in Figure 3E, a similar ratio of excitatory and inhibitory neurons tended to be present across island sizes, and overall the cell density was quite stable irrespective of the amount of space available to the neurons for growth (Figure 3F). The presence of normal neuron morphology was also assessed (Figure 4E) by filling neurons with the Alexa-488 fluorescent dye using a patch pipette, and imaging at 40x or 60x to visualize sub-processes of dendrites and axons. Processes were checked for normal elaboration, branching, and spine formation. Presynaptic terminals were also labeled with synapsin I and juxtaposed with excitatory and inhibitory dendritic markers to verify connectivity between different cell types.

Figure 3. Neurons on micropatterned islands exhibit robust structural and functional properties.

(A) Isolated squares contain neurons, as identified by DAPI-labeled cell bodies stained for the neuronal marker MAP2.

(B) A higher magnification view reveals a heterogeneous mix of DAPI-labeled cells with and without co-expression of MAP2 and the synaptic marker VGLUT1, indicating that both neurons and non-neuronal glial support cells are present and that synaptic connections have formed between the neurons.

(Ci) The presence of synaptic connections, further elucidated with the presynaptic marker synapsin I which appears as localized puncta along neuronal dendrites.

(Cii) Functional activity at synapses verified using the optical marker FM1-43.

(D) Immunolabeling with α-CaMKII and GABA to label the full extent of excitatory and inhibitory cell bodies and dendrites. Cell bodies can be visualized as bright puncta relative to diffuse dendritic staining, and the occurrences of these somata can be counted manually while panning around the square with the imaging system.

(E) A similar ratio of excitatory and inhibitory neurons tended to be present across island sizes.

(F) Neuron cell density remained stable across squares of the same chip irrespective of the amount of space available to the neurons for growth.

(G) Action potentials recorded intracellularly for neurons in either small islands (left traces) or large islands (right traces).

(H) Overall, neurons across a variety of micropatterned islands exhibit comparable functional activity, suggesting that our culturing procedure results in non-pathological function in the networks under study.

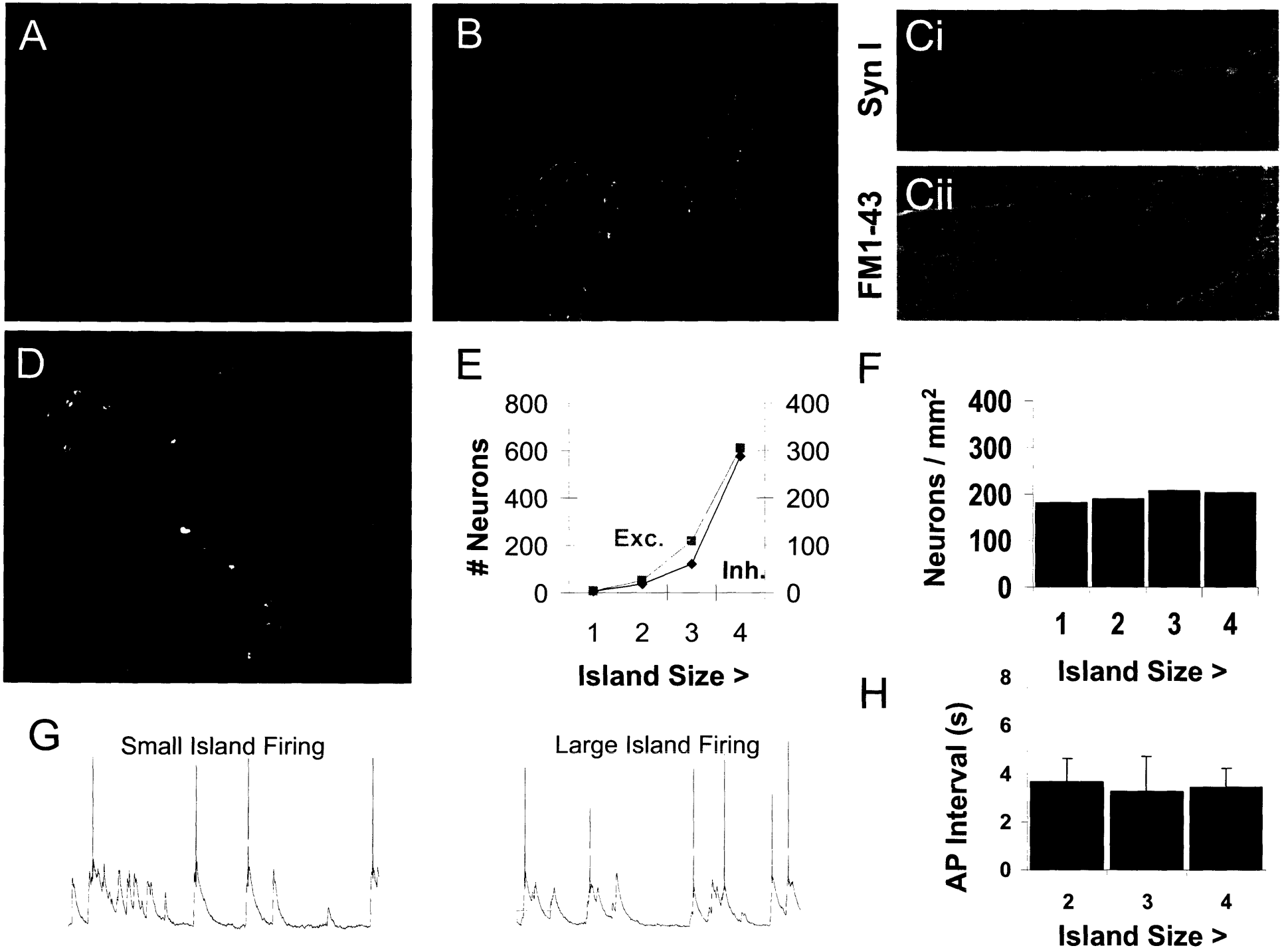
A
B
Ci
Syn I
Cii
FM1-43
D
E
800
600
400
200
0
400
300
200
100
0
Neurons
Exc.
Inh.
1
2
3
4
Island Size >
F
Neurons / mm2
400
300
200
100
0
1
2
3
4
Island Size >
G
Small Island Firing
Large Island Firing
H
AP Interval (s)
8
6
4
2
0
2
3
4
Island Size >

Finally, electrophysiological properties were compared in neurons across islands of different sizes. Passive membrane properties and resting membrane potential were intact across cells (data not shown) and action potential spiking frequencies were on average the same irrespective of island size, though the very smallest island (Island 1) did not present enough neurons for a functional analysis. Thus neurons across a variety of micropatterned islands exhibit comparable functional activity, suggesting that our culturing procedure results in non-pathological function in the networks under study.

Implications of stable network activity despite variations in network size

While neurons in islands of different sizes exhibited stable degrees of activity (Figure 3G), the number of neurons contributing to that activity was dramatically different from one island to the next (Figure 3E). Since cultured neurons lack input from exogenous sources, the level of activity in cultures is dictated by the number of neurons that spontaneously fire, which is in turn influenced by the summation of synaptic release events, which is calculated from the number and strength of those events. For a small number of neurons to consistently fire at the same rate as a large number of neurons thus means that they either 1) have the same number of synapses providing depolarizing input as their larger-network counterparts, or 2) have fewer inputs due to having fewer synaptic partners, but the inputs that they do have are stronger and thus provide more depolarization. In either case, an interesting mechanism seemed to be at work to ensure that firing rates were preserved in these networks of dramatically different size.

Note: More alternative mechanisms that could contribute to a stable firing rate include 1) changes in inhibition or 2) a change in channel properties such as a reduced threshold for voltage-gated sodium channel activation, these caveats are discussed later.

Changing network size changes structural synaptic capacity

Changing the number of neurons that are available to provide synaptic partners could change the number of synapses formed by each neuron. To distinguish whether networks of different sizes result in a different number of synaptic connections per neuron, I performed immunostaining for synapsin I (Figure 4A), which labels presynaptic terminals in localized puncta that can be easily counted. For this and the

Figure 4. Scaling network size changes structural synaptic capacity.

(A) Immunostaining for synapsin I to count the number of presynaptic terminals.

(B) Synapse density was significantly increased on the larger island, despite a constant neuron density between large and small islands (Figure 3F), indicating that neurons in the larger networks form more synapses with one another.

(C) Immunostaining for α-CaMKII to quantify the % area occupied by excitatory dendritic branches.

(D) Branch density was significantly increased on the larger island, despite a constant neuron density between large and small islands (Figure 3F), indicating that neurons in the larger networks interact via larger dendritic trees.

(E) Live imaging 15 minutes after filling of neurons with the fluorescent dye Alexa 488 to label neuronal morphology.

(F) Single neuron dendrite area was increased on the larger island, particularly in terms of the length of the proximal branch.

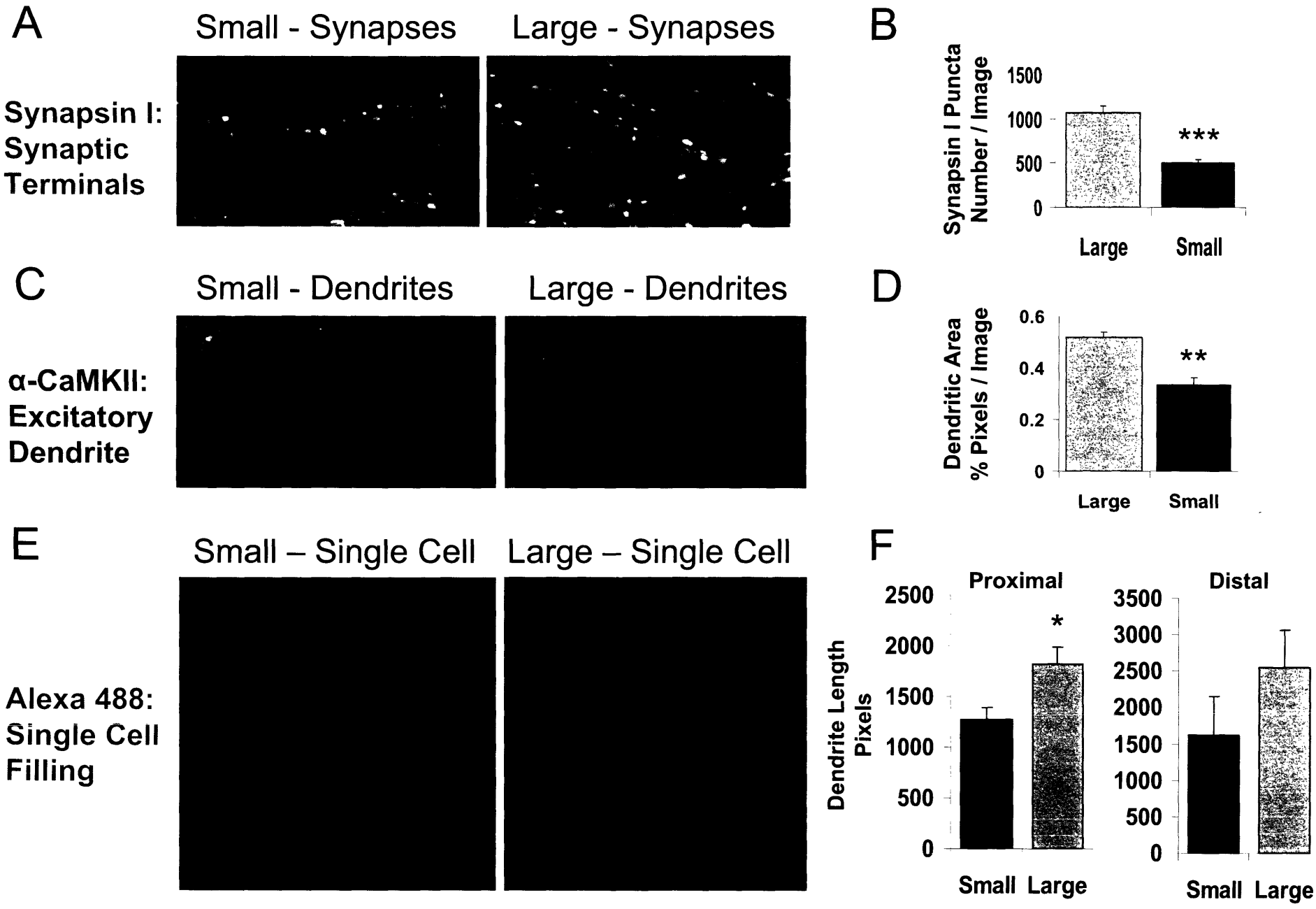
A
Small - Synapses
Large - Synapses
Synapsin I:
Synaptic
Terminals
B
Synapsin I Puncta
Number / Image
1500
1000
500
0
***
Large
Small
C
Small - Dendrites
Large - Dendrites
α-CaMKII:
Excitatory
Dendrite
D
Dendritic Area
% Pixels / Image
0.6
0.4
0.2
0
**
Large
Small
E
Small – Single Cell
Large – Single Cell
Alexa 488:
Single Cell
Filling
F
Proximal
Distal
Dendrite Length
Pixels
2500
2000
1500
1000
500
0
*
3500
3000
2500
2000
1500
1000
500
0
Small Large
Small Large

remaining quantifications, we focused our comparisons on a "Large" island (Figure 3, Island 4) vs. a "Small" island (Figure 3, Island 2). Here, even though a given region of space was constant for neuron density between large and small islands (Figure 3F), it was dramatically increased for synapse density on the larger island (Figure 4B), indicating that neurons in the larger networks form more synapses with one another. The capacity to accomplish these connections may be partially provided by somewhat larger dendritic trees per neuron, as both the overall density of dendrites in the images was increased for large networks (Figure 4C-4D) and the dendritic tree measured by filling with Alexa 488 for single cells was larger (Figure 4E-4F).

The dendrites were likely larger in part because they had more room to grow in the larger islands, or perhaps due to an impetus to grow larger in response to synaptic activity (Sin et al., 2002) - it should be noted that in many cases neurons in the middle of the smaller islands expressing smaller dendrites did not fill all of the room available to them to potentially grow. In any case, whether due to a larger dendritic tree or a general proliferation of synaptic connections, larger networks were characterized by neurons forming more synaptic connections with their surrounding partners than their counterparts in smaller networks.

Scaling network size changes unitary strength per synapse

Again, for a small number of neurons to consistently fire at the same rate as a large number of neurons thus means that they either 1) have the same number of synapses providing depolarizing input as their larger-network counterparts, or 2) have fewer inputs due to having fewer synaptic partners, but the inputs that they do have are stronger and thus provide more depolarization. The results of Figure 4 indicate that the smaller networks did not sustain the same number of synapses as the larger ones, and we were thus interested to see whether they compensate for their reduced number of synapses by imparting more strength to each one.

Our current knowledge of neuronal homeostatic processes (Turrigiano et al., 1998; Turrigiano and Nelson, 2000) suggests that neurons do initiate active processes that seek to maintain a constant amount of total input synaptically. If this is the case, then cells in which synapses are more numerous may allocate a reduced amount of synaptic efficacy to each one, such that a small number of strong synapses is substituted

for a large number of weaker synapses. We were thus prompted to elucidate potential differences in functional connectivity in our networks of different sizes.

We first sought to measure quantal size, or the amplitude of AMPA receptor-mediated miniature excitatory postsynaptic currents (mEPSCs, Figure 5A). Cells were patched and voltage clamped at -60 mV in the presence of TTX to discourage synchronous release. Under this recording configuration all measured postsynaptic responses involved the transmission of single vesicles, such that we had an accurate measure of quantal synaptic strength independent of other parameters such as probability of release. Excitatory quantal size in small networks was markedly increased compared to mEPSC amplitude in large networks (Figure 5B). However, mEPSC frequency was not significantly different in the two types of networks (Figure 5C), despite a reduced number of synapses in the small network (Figure 4A). We interpret this as a difference in the number of vesicles per synapse, that could be upregulated in the small network in consort with quantal size, to compensate for a reduced number of functional synapses.

Scaling network size changes the functional coupling between pairs of neurons

Given that the strength of individual synapses seemed to be increased in connections between neurons in the smaller network, we also wished to assess the full functional connectivity from one neuron to the next. If cultured neurons experience a different number of potential synaptic partners, then they may couple functionally with those partners to different extents. The extent to which pairs of neurons were functionally coupled was assessed via evoked synaptic transmission using dual intracellular patch clamp (Figure 5D). Action potentials were elicited in one "presynaptic" neuron while the synaptic response was measured in voltage clamp in the second "postsynaptic" neuron. Typical evoked transmission in large networks (Figure 5E, top trace) was significantly reduced compared to similar transmission in small networks (Figure 5E, bottom traces), a trend that was maintained across many paired connections (Figure 5F). It should be noted that Figure 5F does not include for quantification pairs in which evoked transmission in one neuron single-handedly triggered an action potential in the postsynaptic neuron, as such depolarizations were too large to quantify in voltage clamp with our amplifiers. Interestingly, while such

Figure 5. Scaling network size changes unitary strength per synapse and the functional coupling between pairs of neurons.

(A) mEPSCs were recorded postsynaptically via whole cell patch clamp in the presence of TTX in either a large or small network.

(B) Average mEPSC amplitude for neurons recorded in each size network shows an increase in mean event amplitude in small networks relative to larger ones (*, $P < 0.001$ unpaired t-test).

(C) Average mEPSC frequency for neurons recorded in each size network. mEPSC frequency was not significantly different in the two types of networks, despite a reduced number of synapses in the small network (Figure 4A)

(D) The extent to which pairs of neurons were functionally coupled was assessed via evoked synaptic transmission using dual intracellular patch clamp. Action potentials were elicited in one "presynaptic" neuron while the synaptic response was measured in voltage clamp in the second "postsynaptic" neuron.

(E) Typical evoked transmission in large networks (top traces) was significantly reduced compared to similar transmission in small networks (bottom traces) (note different scale bars).

(F) Quantification for all evoked transmission in large and small networks. Evoked responses in small networks were significantly larger than evoked responses in large networks. Note: Pairs in which evoked transmission in one neuron single-handedly triggered an action potential in the postsynaptic neuron were omitted, as such depolarizations were too large to quantify in voltage clamp with our amplifiers. While such presynaptically induced spiking was rare in large networks, it was relatively common in small networks.

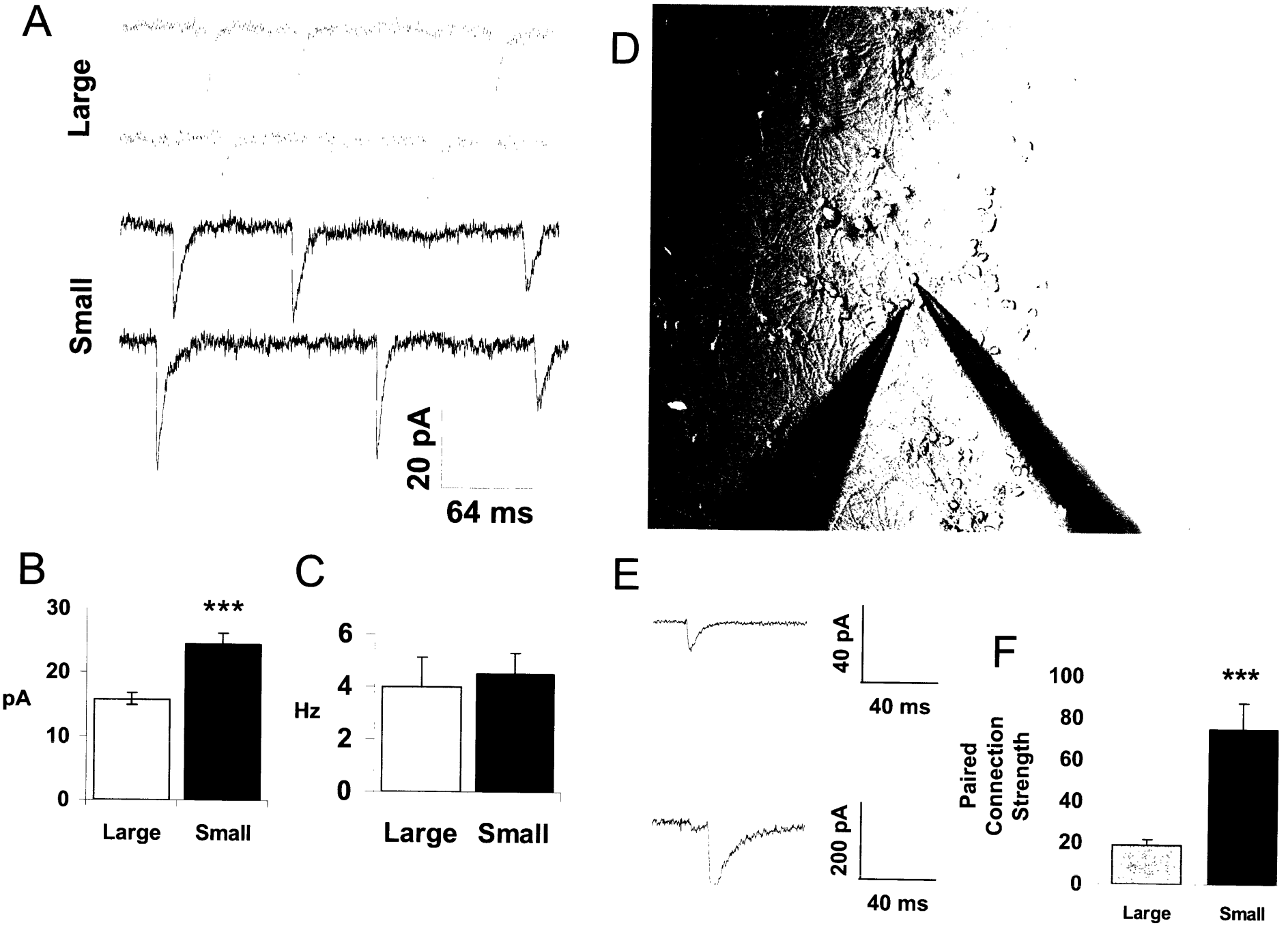
A
Large
Small
20 pA
64 ms
D
B
30
20
10
0
pA
***
Large
Small
C
6
4
2
0
Hz
Large
Small
E
40 pA
40 ms
200 pA
40 ms
F
Paired Connection Strength
100
80
60
40
20
0
***
Large
Small

presynaptically induced spiking was rare in large networks, it was relatively common in small networks.

The strength that a given neuron allocates to its partner is indicative of how each neuron chooses to distribute its connectivity – interpreting degree of connectivity as a function of number of available partners is useful for considering the possibility that each neuron has a finite amount of synaptic resources that can be allocated (Fonseca et al., 2004).

Scaling network size changes functional network architecture and excitatory-inhibitory balance

Evaluating how networks of different sizes use synaptic connectivity to stabilize their firing rates could require a more subtle examination than simply examining the number of synaptic junctions (Figure 4). Synapses enable conductance by which charge can pass from one neuron to the next, and thus their strength and number can be regulated to control the flow of this charge. However, charge can also be regulated by the neuron by selecting the *identity* (excitatory / inhibitory) and *target* (excitatory / inhibitory) of these synaptic junctions as they are expressed. We thus hypothesized that additional stabilization of network firing could result from a reconfiguration in the identity and targeting of synaptic connections, to modulate the functional value of available synaptic contacts.

To evaluate the relative balance of excitatory and inhibitory connections that were formed in our networks, we first immunolabeled for α-CaMKII to restrict our analysis to excitatory dendrites for simplicity. We then used the markers VGLUT1 (excitatory) and GAD65 (inhibitory) to label the synapse type onto these excitatory dendrites in large vs. small networks (Figure 6A). Interestingly, we observed that the ratio of excitatory and inhibitory synapses along a given length of excitatory dendrite was maintained at a constant level from one size network to another (Figure 6B). However, the relative size and intensity of the two forms of synapses as measured by the integrated optical density (IOD) was scaled in the small networks relative to the larger ones to favor excitatory synapses (Figure 6C). Interestingly, most of this shift in ratio was due to a significant decrease in the size of inhibitory synapses in the small networks (data not shown).

Figure 6. Scaling network size changes functional network architecture and excitatory-inhibitory balance.

(A) Triple immunostaining for the excitatory dendrite marker α-CaMKII, the excitatory synapse marker VGLUT1, and the inhibitory synapse marker VGAT.

(B) Ratio of excitatory and inhibitory synaptic densities per unit length of dendrite. There is no significant difference in the relative density of E / I synapses between large and small networks.

(C) Ratio of excitatory and inhibitory synaptic intensities per individual synapse. The relative size and intensity of the two forms of synapses as measured by the integrated optical density (IOD) was scaled in the small networks relative to the larger ones to favor excitatory synapses. Most of this shift in ratio was due to a significant decrease in the size of inhibitory synapses in the small networks (data not shown).

(D) Triple immunostaining for the excitatory dendrite marker α-CaMKII, the inhibitory dendrite marker GABA, and the excitatory synapse marker VGLUT1.

(E) Density of excitatory synapses made onto either an excitatory or inhibitory dendrite in large or small networks. A significant reduction of excitatory synapses onto inhibitory dendrites is observed in small networks.

(F) Excitatory synaptic intensities per individual synapse on either excitatory or inhibitory dendrites. There is no significant difference in excitatory intensity onto either type of postsynaptic cell between large or small networks.

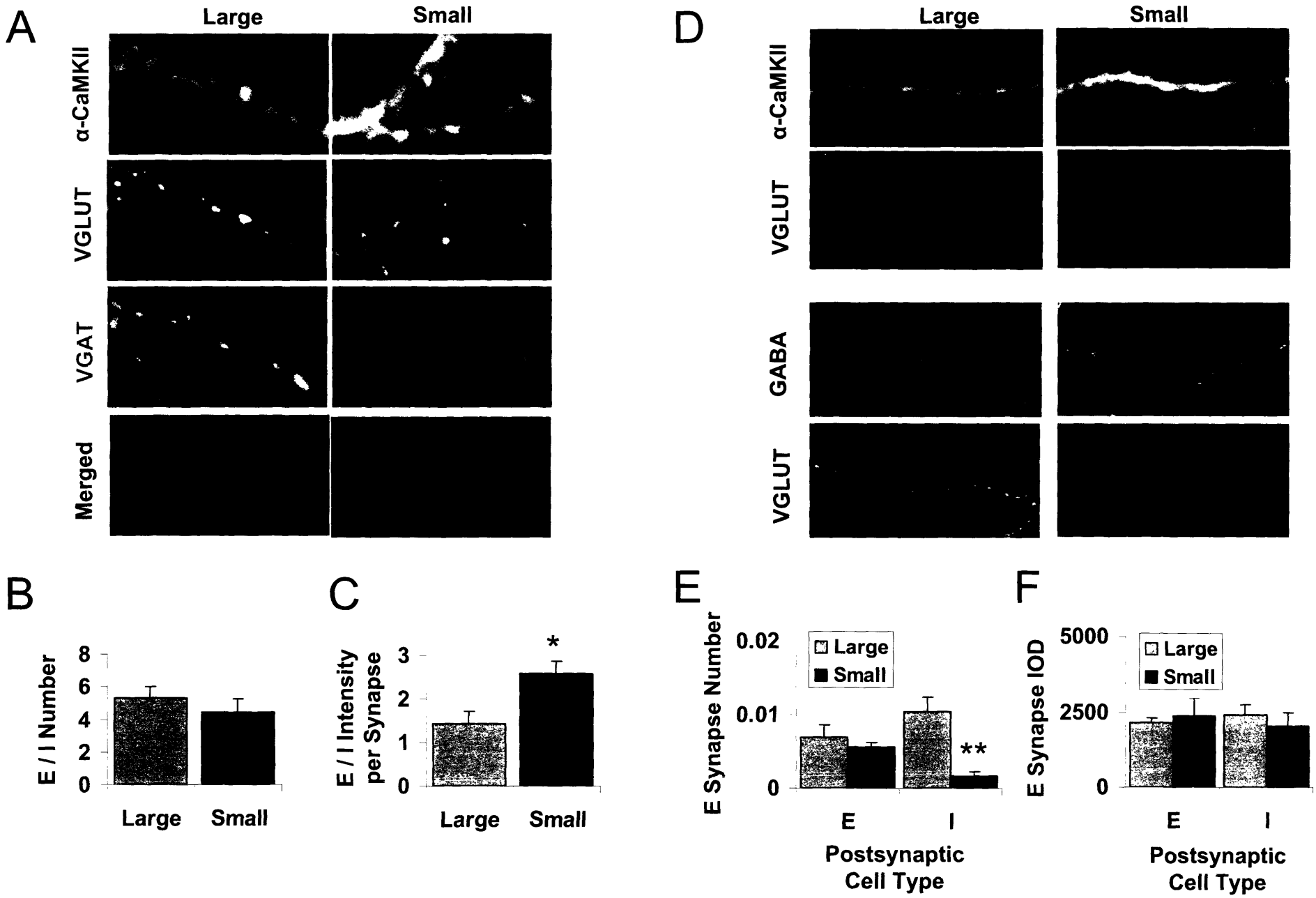
A
Large
Small
α-CaMKII
VGLUT
VGAT
Merged
D
Large
Small
α-CaMKII
VGLUT
GABA
VGLUT
B
E / I Number
8
6
4
2
0
Large
Small
C
E / I Intensity per Synapse
3
2
1
0
*
Large
Small
E
E Synapse Number
0.02
0.01
0
Large
Small
**
E
I
Postsynaptic Cell Type
F
E Synapse IOD
5000
2500
0
Large
Small
E
I
Postsynaptic Cell Type

Another interesting reconfiguration occurred upon examining the targeting of excitatory projections to either excitatory or inhibitory neurons. Postsynaptic target type was distinguished using CaMKII (excitatory dendrite) and GABA (inhibitory dendrite), while the excitatory terminals themselves were identified and counted using VGLUT1 (Figure 6D). Here, the most notable difference between large and small networks was not in the intensity of the synaptic terminals on the different types of postsynaptic cell (Figure 6F), but on their number. Specifically, excitatory projections onto inhibitory neurons were massively retracted in the smaller networks (Figure 6E), suggesting a dis-inhibition of the networks that could facilitate network activity by reducing the functional drive to inhibitory sub-circuits.

DISCUSSION

This work directly demonstrates an interesting phenomenon – that as the size of a functional network of hippocampal neurons is increased, measures are taken on the part of neurons and their connectivity to maintain a stable level of overall activity. Mechanisms that contribute to this stabilization do not include balancing changes in synapse number, but are rather due to compensatory changes in unitary synaptic strength, more focused connectivity between cells, and a retraction of excitatory drive from inhibitory cells. Speculatively, such effects could suggest that an additional utility of homeostatic processes lies in scaling the efficacy of inputs to appropriately reflect the "relevance" of those inputs to the target neuron, with respect to all of the other neurons that are providing input. In other words, a given contact is less important if there are many other contacts to integrate, and should be scaled as such if information is going to be maximally interpreted and overload avoided.

Another important component of total synaptic efficacy which could be subject to scaling is the probability of release (Murthy et al., 2001) and this could be measured directly in our cultures. Detailed methods for quantifying Pr using optical measures with FM dyes have been developed elsewhere (Ryan et al., 1996; Murthy et al., 1997; Murthy and Stevens, 1998) and refined in our lab (Slutsky et al., 2004). The protocol will allow us to count the number of presynaptic vesicles turned over by a fixed number of action potentials. By comparing this number in small and large cultured networks, we can see if the average likelihood for a given action potential to release a vesicle has changed, providing a direct measure of the activity-dependent probability of release. A

pending development that has inhibited this experiment thus far is the development of micropatterning on fully translucent substrates that can facilitate live imaging. However, we have recently made progress in stabilizing patterns on PDMS substrates, which could provide the visibility that we need.

Such visibility would also enable a particularly interesting set of experiments based on a method also refined in our laboratory (Slutsky et al., 2004), which allows for optical measurements of synaptic plasticity in response to theta-burst stimulation (30 bursts, each containing 5 action potentials at 25 Hz, 500 ms interburst interval). In this case, the number of vesicles released before and after stimulation will be used as a proxy to the strength of synaptic transmission before and after potentiation. The probability of release will be assessed as above, but it will be assessed twice: once before theta burst stimulation, and again 30 minutes after TBS. It will thus provide some measure of resilient changes in synaptic efficacy, and this measure will be compared between networks with different numbers of synaptic partners to determine whether the other observed changes in synaptic properties are accompanied by changes in aggregate synaptic plasticity.

Considering synaptic plasticity as a function of network size is particularly interesting in the context of synaptic scaling. Hypothetically, it could likely be that the neurons in the small network do what they can to preserve their first metabolic function, which is the propagation of action potentials, but only achieve this through the functional tradeoff of impaired plasticity. The smaller networks exhibit significantly stronger quantal responses, and strong quantal transmission is known to be inversely correlated with functional plasticity in hippocampal neurons (Bi and Poo, 1998). Similarly, if the smaller networks do scale up the number of vesicles available for probability of release as could be suggested by our data on mEPSC frequency (Figure 5C), then a high probability of release is also known to be inversely correlated with functional plasticity in hippocampal neurons (Slutsky et al., 2004). Pending experiments will help to identify whether these changes in properties of synaptic transmission are accompanied by implications for the synapse and cell's capacity for plasticity.

CHAPTER 3

Measuring Dynamics Between the Strengths of Multiple Synapses in Cultured Hippocampal Neurons

SUMMARY

While a great deal of work has been done to establish how synaptic transmission involving two neurons occurs and how it changes, much less is known about the dynamics of synaptic transmission involving many neurons (3 or more). Interesting properties may occur at this level, for example how multiple inputs converging on a dendritic tree are led to compete, cooperate, and otherwise interact in response to specific patterns of activation to encode and refine information.

To begin to study these properties, I sought to create a system able to elicit synaptic transmission from multiple input neurons while recording individual synaptic currents postsynaptically. It would be similar to the multi-site iontophoresis technique developed in our laboratory, except that it would also involve the presynaptic element in the transmission event, to bring into play the full mechanism of synaptic transmission and plasticity-associated signals. Multiple inputs could then be stimulated in arbitrary spatiotemporal patterns, synchronously, asynchronously, or sequentially, in order to study principles of how information is encoded across multiple inputs at the cellular level.

The work presented here describes early progress towards this end, in which networks of cultured hippocampal neurons can be stimulated at multiple sites to activate convergent synaptic inputs on single neurons. Such networks exhibit a capacity to change their connectivity in response to such stimulation, and responses of individual synaptic pathways as a result of focal stimulation can be assessed.

INTRODUCTION

One of the most remarkable properties of nervous tissue is its ability to evolve meaningful circuits out of unrefined connections, using only a small allowance of input as a guide. Central neurons seem to be equipped with endogenous mechanisms for refining synaptic efficacy in an activity-dependent manner that is responsive not only to the local activity of the individual synapse, but also that of common inputs across the dendritic tree that provide a context of what other information needs to be simultaneously considered in order to store information to the neuron and improve its comprehension of the surrounding world. These interactions between convergent presynaptic inputs on a common postsynaptic neuron are likely to hold relevance for our

understanding of the nature of associative learning, both in terms of constraints and special abilities. The purpose of this body of work has thus been to take some initial steps towards an experimental method for exploring basic interactions between multiple inputs on target cells in cultured networks of central neurons.

Such interactions have already begun to be examined in the peripheral nervous system. Here, motor neurons compete for control over muscle fibers (Balice-Gordon and Lichtman, 1993), just as central neurons compete for downstream connections. In the neuromuscular junction (NMJ), the competition intensifies until a single axon has won (Jansen and Fladby, 1990), with winners gradually accumulating more area and a corresponding increase in synaptic strength (Colman et al., 1997). Eventually, the losing axons fall away, and even their residual postsynaptic terminals are deconstructed (Culican et al., 1998). The struggle thus involves some sequence of events and signals that transitions the system from poly-innervation to a more refined single-innervation.

The role of activity in refinement processes has also been characterized in the neuromuscular junction. Activity seems to be necessary for synaptic elimination, as application of alpha-bungarotoxin prevents elimination (Balice-Gordon and Lichtman, 1994). However, it is not activity alone that is important, but rather specific patterns of activity. For example, while asynchronous inputs tend to engage competitive elimination, synchronous ones prevent it (Busetto et al., 2000).

The situation at the NMJ thus serves as an accessible analogue for long-posited competitive interactions at central synapses (Purves and Lichtman, 1980). Many such interactions exhibit phenomenology similar to the NMJ. For example, in the competition between mammalian eyes for cortical space, functional organization proceeds in an activity-dependent manner (Wiesel, 1982). As described above, blocking activity in the zone of competition also blocks organization (Stryker and Harris, 1986; Hahm et al., 1991). And as above, shifting levels of activity to favor one competing eye puts the other at a territorial loss (Chapman et al., 1986). Finally, synchronizing binocular input prevents territory segregation (Weliky and Katz, 1997), just as it does in the NMJ.

Unfortunately, even in highly characterized systems such as the retinotectal projection of frogs or the retinocortical pathways of mammals, a causal relationship between activity and circuit refinement has been noted, but not explained. The goal of the following methods is therefore to contribute work to extend some of the convenience achieved at the neuromuscular junction to studies at central synapses, in

the hopes of supplementing a phenomenological understanding of activity-dependent heterosynaptic interaction with a mechanistic one.

RESULTS

A multi-electrode interface for cultured neurons

Cultured hippocampal networks can be interfaced to a device capable of presenting electrical stimulation to multiple, discrete locations

My goal was to create an interface for connecting electrically to a network of cultured neurons at multiple sites. Such an interface was intended to allow for the discrete stimulation of individual neurons within the network, and was to be non-invasive so as to permit repeated patterns of stimulation to be applied over long time courses without damaging the network.

Three general methods seemed feasible for focally stimulating neurons: A) photoconductive substrates: making a semi-conductive surface and then changing the conductance of local regions of that surface by using a laser to focally excite a small region of the substrate, B) laser uncaging: using a laser to chemically transform and activate a subset of molecules within the blast radius, where those molecules are known to excite neurons (i.e. glutamate), or C) bringing electrodes close enough to neurons to stimulate them discretely and independently. I opted for method (C) since that was the one that seems most promising for stimulating multiple sites in parallel: (A) and (B) require a laser that could only excite one region of the network at a time. Though in principle one could assemble a "multi-laser" stimulation device, a "multi-electrode" stimulation device seemed more intuitive and cost-effective to program and use.

I thus sought to bring a number of electrodes into close contact with a cultured neuronal network. Since our cultures are two-dimensional in nature, we ideally would wish to bring a single plane of electrodes to bear on the culture. The easiest way to do this was to embed the electrodes in the culture's coverslip. Numerous resources existed on MIT's campus for performing the micro-machining that would be required to do this, and commercial contacts were also established with leading distributors of multi-electrode arrays, such as Panasonic (USA) and Multi-Channel Systems (Germany).

These collaborations provided the multi-electrode substrates upon which all of the remaining aims were actualized.

Hippocampal cultures were prepared on these multi-electrode devices by covering the chips with a thin layer of matrigel, and otherwise adhering to the culture protocols defined in the earlier sections. Once networks had developed and neurons had fully extended processes and formed synaptic connections, confocal microscopy and electrophysiology were used to verify that cultures were healthy and did not appear structurally or functionally pathological. Particular attention was paid to cell density, synapse density, and functional vesicle turnover. Electrophysiological measures, in turn, included intracellular recordings of excitatory and inhibitory synaptic currents, and comparisons of action potential frequencies to those on non-electrode substrates. The purpose of all of these measurements was to establish that the presence of the electrodes embedded in the substrate does not lead to biological changes in the cultured tissue that could impact the relevance of findings in the later experiments.

Electrical stimuli delivered through this interface evoke action potentials within neurons, and do so in a localized manner

The multi-electrode array chips that we used came equipped with micro-machined leads that could be connected to wires, which in turn could be interfaced with custom electronics. The chips also included a series of ground electrodes scattered around the four corners of the culture surface, which could also be accessed electrically. Thus, to drive current through these electrodes, I connected pairs of wires to different analog stimulus isolators (A-M Systems, Model 2200, for example), connecting one wire to the electrode that I wished to stimulate, and the other wire to ground. I then used a computer to specify the waveform that was delivered to the isolator, while "listening" for its effects using an intracellularly patched neuron that was situated nearby to the electrode of interest. With this simple feedback loop in place, I could create a simple program that gradually ramped up the magnitude of the stimulus until it was detected first in fluctuations in the signal acquired at my recording electrode, and second in the spiking of the neuron itself. Assuming that the neuron was close enough to the electrode, some amount of threshold current was sufficient to depolarize the neuron beyond the level of its spiking threshold, at which point the neuron would be effectively stimulated to fire. Additional patches were acquired on other nearby neurons to examine the distance at which different magnitudes of stimulation were able to "reach" the neuron through the charge of the bath to elicit firing.

An alternative means of verifying that we were effectively stimulating neurons was to use the same planar electrodes as recording devices, to pick up the firing of neurons in response to the stimulation of neurons at other sites. Multi-channel amplifiers and recording systems were beginning to emerge on the market through the vendors mentioned above, and it was possible to acquire one of these systems to make use of it for simultaneous stimulation and recording across multiple sites of the cultured network. Ultimately, however, direct intracellular patch clamp provided the most accurate picture of the stimulus-response profile in our electrode to neuron interface.

Multiple synaptic inputs can be evoked to converge on the same dendritic tree

Synaptic transmission can be evoked from one neuron extracellularly to another recorded intracellularly

This step involved using the stimulation method refined in (A), except this time recording a neuron intracellularly that is different from the one being stimulated, to show that we can elicit synaptic transmission. In this case it was necessary to "feel around" for neurons that might be connected to the neuron that we are recording, and this was done by swapping which pair of leads was connected to the stimulator. The leads swapping could be done either manually or with the help of a circuit board and toggle switches.

Whether a neuron had been successfully stimulated was detectable postsynaptically by recording the neuron's activity in voltage clamp and awaiting synaptic input, either listening at -60 mV for excitatory input, or 0 mV for inhibitory input. An effective strategy was to start with a very strong stimulus that is certain to excite surrounding neurons, and then reduce the input until a single neuron is being stimulated to spike a single time. By achieving this, we demonstrated that synaptic transmission could be triggered and recorded through the use of our multi-electrode device.

Multiple sites can be stimulated to evoke distinct synaptic outputs converging onto a single postsynaptic cell

This step used the procedure in the prior step, except repeating it two or more times. Once an intracellular recording with a cell has been established and postsynaptic currents were being recorded in voltage clamp, an evoked connection was established using one of the electrodes of the device to stimulate a neighboring neuron that projects to our recorded neuron. Once that connection was evoking reliably, we could repeat the search process characterized above to locate another synaptic connection impinging on the same neuron.

Inputs can be stably recorded and quantified over time

This method is only useful for characterizing transmission if that transmission is stable over time. Once two or more inputs had been established, they were thus stimulated alternately at ~0.1 Hz to ensure that they did not interact in the same biological time window, and the stability of their efficacy could be assessed. The amplitude of the postsynaptic current that each one elicited was plotted as a function of time, and it was assessed for use-dependent depression or potentiation over a time course of 30 minutes. If a change in synaptic efficacy was observed, then the interval between stimuli should be increased until they are infrequent enough to not change the connection strength significantly. By the same token, if a shorter interval could be used without changing the connection strength, then this could be enacted for more efficient data collection in later experiments.

The introduction of more complex spatiotemporal stimulation to trigger network-wide plastic changes

Multi-site stimulation can be interfaced with real-time computer control for rapid and complex spatiotemporal stimuli

In the above goals, deciding which electrodes of the array get stimulated is accomplished by manually switching the leads connected to a stimulation device, or at best using manual switches or buttons to enable the toggling. A shortcoming of this method is that which electrodes are active can only be changed as quickly as the human operator can move, and there may be phenomena or interactions between inputs that occur on very fine time scales (10 ms, for example) that would be difficult to initiate manually with any degree of reliability.

One solution is to place the switching under computer control. Stimulation could be applied to all of the pins, but only the pins that the computer enables would receive it. The decision would be made at the level of relays, which when closed enable the current to pass, but when open prevent the electrode from being stimulated. The relays could then be opened and closed using a series of digital signals from a computer controlled by simple logic translated from commands delivered via a standard I/O port.

For the relays in question, we used photo-MOS integrated circuits (NAIS AQW series), which make use of an optical switching system: the input command modulates an internal LED, which shines light on a photodiode connected to the output terminals. We used a normally-open configuration such that the LED must be triggered by active input in order for the relay to be closed, and once the input has ceased the relay will return to an open state. The use of an ~500 Ω resistor drew 1 mA of current from the digital signal, and enabled the relays' switching after an approximately 0.5 ms ramp-up. This timeframe was sufficient for "turning on" the electrodes in advance of the stimulus delivery, at an interval that was appropriate for investigating fast heterosynaptic interactions.

For controlling these relays, one relay was deployed for each of the electrodes that we wished to gate, and each required its own digital command signal. The digital command signals were delivered by Intel 8255 peripheral chips, each of which were capable of providing 24 output pins to control 24 relays. The input to the 8255's determined which of these pins was activated with the digital signals needed to close the

relays. Each 8255 was thus fed words of data to decode, from a standard microcontroller (Intel 8051). The 8051 in turn communicated directly with the computer via a standard I/O interface (serial / RS232 port). A communications protocol was initially developed in Hyperterminal, a standard communication program installed by default with all Windows computers, and then adapted to Matlab or C++ where a graphical user interface was constructed. The end goal was thus a software-enabled delivery system of time sequenced commands, analogous to the "cues" on a theater-company lighting board, for which gates are activated at each delivery clock cycle, to determine with high speed resolution which electrodes are able to conduct the stimulus.

Multi-site stimulation can elicit plastic, long-term changes in a cultured neuronal network

The purpose of this system was to explore heterosynaptic dynamics in cultured neuronal networks. A critical question for the experiments that the above system could enable is whether cultured networks are imbued with the capacity for plasticity. Recent work in our lab has established that while plasticity protocols are often difficult to replicate in dissociated culture, pre-incubation with treatments that up-regulate NMDA receptors can restore plasticity to the dissociated neurons (Slutsky et al., 2004). Had our stimulation protocols fail to elicit plastic changes in our cultures initially, these new culture conditions can be applied to provide plasticity or facilitate existing plasticity. Plasticity of individual synaptic connections was assessed using either high frequency stimulation to the presynaptic neuron alone (theta-burst stimulation), paired stimulation to the pre- and post-synaptic neurons (Bi and Poo, 1998), or paired stimulation between two presynaptic neurons. This capacity for plasticity experiments, established in a system that offers control over multiple synaptic pathways, offers an exciting array of possibilities for exploring how multiple synapses interact to effect the stabilization of activity patterns.

DISCUSSION

With the ability to establish and stimulate isolated inputs into single neurons, the principles discussed here provide a direct means for measuring and altering functional synaptic connectivity. The following section discusses the immediate potential for reducing these principles to practice, both in terms of an additional method that could provide important information, and a discussion of the types of experiments to which such an assay could be used.

Assessing Structural Correlates of Functional Connectivity

An important consideration will be how to locate a functional input of interest on the dendritic tree. This will likely occur when one is asking where a given input is targeting to with respect to another input, or whether multiple synapses from a single input are relatively concentrated on the dendrite or diffusely segregated. In any case there will probably be the need to locate and distinguish at least two pools of synapses. Such a method could be provided by FM functional staining in conjunction with focal stimulation. The styryl dyes FM1-43 and FM4-64 fluoresce green and red, respectively. These dyes are used commonly to stain the presynaptic terminals of functional synapses (Betz and Bewick, 1992; Sala et al., 2001), and bind to the membrane of fusing synaptic vesicles, which are then internalized. To stain a terminal one needs only to trigger the release of its vesicles during bath application of the fluorescent dye.

If the dyes were perfused one at a time, and if vesicle fusion could be restricted to one team's terminals at a time, then the two teams could be demarcated. This could be done by applying extracellular stimulation to one cell group while perfusing the first dye, and then switching to stimulate the second group while perfusing the other dye. The action potentials elicited by the extracellular stimulation would propagate down the axons and trigger vesicle exocytosis and dye uptake. By strongly driving one input at a time while applying that input's color of dye, terminals from each team can be differentially labeled, particularly if executed in low extracellular calcium to reduce spontaneous fusion.

Potential Experiments for Investigation

Questions of Synaptic Organization and Refinement Principles

1. Organization at the level of the single cell: if projections from two inputs occur on the same target cell and are driven asynchronously, is there a dendritic ordering to their occurrence either before or after the patterned stimulation? Do they divide the dendritic tree up, with one input winning one branch and the other input winning a neighboring branch? Might one input hold the distal branches while another controls the proximal? Or is there no organization at all, with inputs intermingling within the same tree, branch, and branchlet?

2. Hebb's Postulate: do neurons that fire together wire together? Could a projection distribution that is initially segregated be made to fuse, simply by synchronizing the activity patterns of the two competing teams? From a postsynaptic point of view, synchronized activity would render both teams indistinguishable. The critical question is whether this synchrony is enough to enforce redistribution.

3. Synaptic Elimination: does it hold at the central synapse? Synaptic elimination predicts that more active inputs will eliminate less active ones. Is it possible for an initially intermingled group of inputs to be made more homogenous, simply by applying a differential amount of stimulation to the two teams? One team could be over-stimulated while the other is not stimulated at all. The critical prediction would be that the non-stimulated team decreases in synapse number, although it is difficult to predict whether this decrease would be across the entire target area, or just in a more localized area of competitive contact.

Questions of Refinement's Activity-Dependence

4. Dependence on Firing: If refinement can in fact be induced, it is natural to ask whether different degrees of refinement can be achieved by different degrees of competitive stimulation. If Hebb's rule is in effect, does more activity, and thus more sample instances for the cell to test for coordination, facilitate better co-wiring? Or if

elimination is operating, does a larger differential in activity lead to stronger revocation? Finally, is activity the only important component, and will silencing it by tetradotoxin dismantle all levels of organization?

5. Dependence on Inhibition: What role does inhibition play in the reorganization of synaptic targeting? Recent evidence suggests that both the gating and balance of cortical refinement, such as that observed in mouse primary visual cortex (Fagiolini and Hensch, 2000) depend on sufficient inhibitory activity. At the same time, interesting aspects of synaptic interactions may occur at the cellular level wholly independently of inhibitory input (Nelson et al., 1994). The importance of inhibition to synaptic refinement and dynamics could be assessed in the above, more tractable system, using the following conditions: 1) application of picrotoxin to block GABA(A) channels, thus terminating inhibition, 2) application of the GABA(A) agoinst muscimol, to enhance inhibition, and 3) GAD65 knockout, to block GABA synthesis and thus inhibition. Muscimol might also be applied in a very small dose, to measure whether even slightly perturbing the balance between excitation and inhibition is enough to disrupt refinement.

6. Parameters of Synaptic Homeostasis: It has been proposed (Turrigiano et al., 1998) that neurons may, in order to keep their overall excitability within a certain range, scale the strengths of all their inputs multiplicatively while maintaining relative levels between their inputs. The relationship of this global property to activity of single or a few inputs can be assessed, and the total amount of activity able to trigger compensatory changes can be assessed. The extent of these compensatory changes can also be assessed by stimulating one set of inputs while monitoring a different set of inputs.

Questions of the Genetic Basis of Synaptic Refinement

7. Genetic Perturbation Experiments: Just as knockout animals are assessed for ocular dominance plasticity, the functional knockout or overexpression of the same molecules might be measured at the synaptic level using the preparation described above. For example, competition paradigms might be applied to constitutively-active, dominant-negative or overexpressed forms of candidate plasticity genes, in order to ascertain the role of those genes in not just macrocellular organization, but synaptic refinement.

8. Co-culture Experiments: The stimulation and competition paradigms described above can be applied to a "mixed culture" of two types of cells plated together. Normal cells could be plated alongside cells from mice with a GFP-tagged knockout mutation. The mutation could involve known mediators of plasticity to determine how these mediators function in the context of synaptic refinement. For example, one competitor pool of neurons could be plated from mice lacking the TrkB receptor for BDNF. These cells could be made to compete against normal cells possessing the receptor, in order for the role of BDNF stabilization in refinement to be directly assessed.

Conclusion

The paradigm proposed above could thus provide a novel assay for the critical molecules and emergent phenomena of synaptic refinement. Additionally, it provides a simplified arena for intercellular competition analogous to the often-used visual cortex, with two additional advantages: 1) convenience, in that the assay does not require the growth, training and maintenance of an animal and 2) accessibility, in that cultured preparations are much more open to methods of visualization, recording and stimulation than *in vivo* models. This preparation facilitates the observation of heterosynaptic interactions at the subcellular level, through the functional characterization, stimulation, and localization of individual synapses between individual cells. It thus takes a step forward in enabling experiments, previously restricted to the large arbors of the neuromuscular junction, and now available to address questions relevant to the functional interaction and refinement of central synapses.

MATERIALS AND METHODS

This work for the most part used widely-applied, conventional techniques for its measurements except for a few exceptions, and these exceptions are detailed in the chapters themselves. In the first chapter, the method for quantifying glutamate release from single vesicles is new, in the second chapter the method of designing lithographic cultured networks is new, and most of the work relating to multi-site stimulation of cultured neurons in the third chapter makes use of unpublished protocols. The remaining protocols used in this work are detailed immediately below.

Cultured Hippocampal Neurons and Transfection

Hippocampi were dissected from postnatal day 1 Sprague-Dawley rat pups and cultured as previously described (Liu et al., 1999). A pCDNA3.1-VGLUT1 construct (Varoqui et al., 2002) was used to transfect cells at 6-11 days in vitro using the calcium phosphate method, with neurons transfected at least two days prior to observation. VGLUT-enhanced neurons were compared to control neurons from the same batches of culture, with evoked recordings age-matched from 9-11 days in vitro, miniature recordings measured at DIV 10, glutamate release experiments performed at DIV 14-16, and activity-dependence experiments at DIV 16 following two days of drug treatment. All experiments involving animals were approved by the Massachusetts Institute of Technology's Committee on Animal Care.

Imaging and Immunohistochemistry

All imaging was performed using an Olympus Fluoview confocal microscope (Olympus, Melville, NY) with a 40× planapochromatic water immersion lens (1.15 NA). Cell cultures were fixed with FSB solution (4% paraformaldehyde and 4% sucrose in 1x PBS) and permeabilized with 0.5% Triton X-100 for 30 min. at 22-24°C. Primary antibodies against VGLUT1 (Chemicon, Temucula, CA), synaptotagmin (American Qualex, San Clemente, CA), or synapsin I (Chemicon) were applied, followed by rinses in PBS and visualization with Alexa 488-, 546-, or 633-conjugated secondary antibodies (1/400; Molecular Probes, Eugene, OR). AM1-43 (Biotium, Richmond, CA) is a form of the FM1-43 styryl dye (Renger et al., 2001), with an

additional aldehyde-reactive amino group at the hydrophilic end rendering it less sensitive to fixation. Coverslips containing cultured neurons were bathed for 120 s at 22-24°C in high K^+ solution (+ 8 μM AM1-43) and placed into Tyrode solution (above, +1 μM TTX) for 15 min. They were then transferred for quenching to the sulfonated b-cyclodextrin derivative ADVASEP-7 (125 μM, Biotium) for 4 min. at 22-24°C. Cells were fixed immediately after staining in FSB (above) and 0.02% glutaraldehyde for 60 min, rinsed in 1x PBS, and blocked with 0.4% saponin and 5% serum in 1X PBS. First and secondary antibodies were then applied as above. All images were collected at 1280 x 1024 pixel resolution and 4X software zoom, using a z series projection of 8 to 11 images taken at 0.8 μm depth intervals. An average image contained approximately 250 synapses.

Whole Cell Recording

Whole cell patch clamp recordings were performed as previously described (Renger et al., 2001). Patch pipettes (3–6 MΩ) contained (in mM) potassium gluconate, 120; KCl, 3; HEPES, 10; NaCl, 8; $CaCl_2$, 0.5; EGTA, 5; Mg^{2+}-ATP, 2; and GTP, 0.3; pH was adjusted to 7.3 with NaOH. Perforated patch pipettes were front-filled with a solution containing (in mM) potassium gluconate, 130; KCl, 4; HEPES, 10; NaCl, 8; EGTA, 0.4; pH was adjusted to 7.2 with KOH, and then back-filled with the same solution containing 150 ng/ml amphotericin B (Sigma, St. Louis, MO). Extracellular solution was based on Tyrode solution containing (in mM): NaCl, 145; KCl, 3; glucose, 15; HEPES, 10; $MgCl_2$, 1.3-2.6; $CaCl_2$, 1.3-2.6; 50 μM picrotoxin (Sigma); pH adjusted to 7.4 with NaOH. Signals were recorded under voltage clamp (-60 mV) using a MultiClamp 700A amplifier (Axon Instruments, Foster City, CA), digitized at 10 kHz, filtered at 1 kHz, and recorded using in-house software. 5 μM 1,2,3,4-Tetrahydro-6-nitro-2,3-dioxo-benzo [f] quinoxaline-7-sulfonamide (NBQX; Sigma) was used to verify AMPA currents. 1 μM tetrodotoxin (TTX; Biotium) was added for mESPC recordings.

Dual-Cell Evoked Recordings

For dual-cell evoked EPSCs, a second whole cell patch or perforated patch was achieved and action potentials were stimulated by injecting 100-300 pA of current over

10 ms (current clamp, Figure 5), or 30-80 mV over 0.5 ms (voltage clamp, Figure 8). For glutamate antagonist experiments, 600 μM γ-DGG (Tocris, Ellisville, MO) was bath-applied. For tuning of synaptic failure rates, varying concentrations of calcium (0.6-1.3 mM) and magnesium (2.6-3.4 mM) were bath applied for each connection until the apparent probability of release was low (0.4-0.1). Data was then collected after a stable baseline at a consistent failure rate was established.

Estimation of the Potential for Multi-Vesicular Release

The potential for multi-vesicular release in our measurements was determined while assuming 1) approximately 10 release sites per bouton (Schikorski and Stevens, 1997) and 2) independent release between vesicles. Binomial statistics were utilized in which the number of vesicles undergoing fusing (N) relates to the probability that a given vesicle will fuse (p) and the number of vesicles able to fuse per bouton (N_{max}). We determined the probability of event failure as the likelihood that zero vesicles could undergo fusion: $P_{N=0} = (1-p)^{N_{max}}$, using observed failure rates to estimate p. The probability of exactly one vesicle fusing would in turn be: $P_{N=1} = N_{max}(1-p)^{N_{max}-1}p$. As such, the probability of multivesicular release would be the likelihood per action potential that there is neither a failure nor a single release, but rather that several vesicles release: $P_{N\geq 2} = 1 - P_{N=1} - P_{N=0}$, or $1 - N_{max}(1-p)^{N_{max}-1}p - (1-p)^{N_{max}}$.

Chronic Drug Treatments of Cultures

In treatments to chronically shift activity levels, cultures were treated continuously beginning at DIV 14 and observed at DIV 16-17. 5 μM 1,2,3,4-Tetrahydro-6-nitro-2,3-dioxo-benzo [f] quinoxaline-7-sulfonamide (NBQX; Sigma), 50 μM DL-2-Amino-5-phosphonopentanoic acid (AP5; Tocris), or 20 μM bicuculline methobromide (Sigma) were used to block AMPA, NMDA and $GABA_A$ receptors.

Synaptic vesicle purification and uptake

Synaptic vesicles were purified from 30 grams of adult rat cerebral cortex (including hippocampus) using the procedure of Jahn and coworkers (Hell et al., 1988) and stored at -80°C until use. Vesicles were thawed on ice and diluted in sucrose buffer (320 mM

sucrose, 10 mM HEPES, pH 7.4) to a protein concentration of 250 µg/ml (Pierce Bradford assay using BSA as a standard). Aliquots (100 µl) were mixed with 50 µl of KCl solution (8 mM) in uptake buffer (110 mM potassium tartrate, 20 mM HEPES, 2 mM $MgS0_4$, pH 7.4) and pre-incubated for 5 min. at 37°C in the presence or absence of the specific inhibitors rose Bengal or Trypan blue. Uptake was initiated by the addition of 50 µl of uptake buffer containing 20 mM Na2-ATP, 0.9 µM 3H-glutamate (NEN; 51 Ci/mmol) and various concentrations of unlabelled glutamate, and allowed to proceed at 37°C for 0.5 to 15 min. To terminate the uptake, tubes were placed in an ice / water slurry and the vesicle suspensions were filtered under vacuum through GF/F filters pre-wetted with uptake buffer, and washed with 8 ml of ice cold uptake buffer. The radioactivity bound to the filter was solubilized in 1 ml of 1% SDS before adding 5 ml of EcoScint scintillation fluid.

VGLUT1 Overexpression and Functional Analysis

Sequences encoding VGLUT1 (GenBank accession # U07609 (Ni et al., 1994)) were cloned (Varoqui et al., 2002) and amplified using a 5' primer containing an EcoRI site (ggaattccaccatggagttccggcaggaggagtttcgg) and a 3' primer containing an SalI site to remove the stop codon (actggtcgaccagtagtcccggacaggggtggggg). Following digestion with EcoRI and SalI, the PCR product was subcloned in frame into pEGFP-N1 to produce a C-terminally EGFP-tagged transporter. The cDNA fusion insert was subcloned into pCDNA3.1 using EcoRI and NotI for transient heterologous expression using the vaccinia T7 hybrid system in PC12 cells as described previously (Varoqui et al., 2002). A light population of membranes containing synaptic-like microvesicles was isolated from VGLUT-expressing PC12 cells and from mock-transfected cells as described (Varoqui et al., 2002). Western analysis was then also performed as described (Varoqui et al., 2002). VGLUT1 transport activity was assessed by measuring ^{3}H-glutamate uptake under optimal conditions (Mg^{2+}-ATP, 5 mM; chloride ion, 4 mM) for 5 min at 32°C in the presence and absence of the H^+-uncoupler carbonyl cyanide m-chlorophenylhydrazone (CCCP, 50 µM) as in earlier studies (Schafer et al., 2002; Varoqui et al., 2002).

Data Analysis

Analysis of electrophysiological data was performed in MiniAnalysis (Synaptosoft, Leonia, NJ), for mEPSCs, and custom scripts written in C++ and MATLAB (Mathworks, Natick, MA) for EPSCs evoked presynaptically and iontophoretically. EPSC failure rates were estimated using a threshold of approximately 4 pA. Such a threshold was also invoked for determining mean amplitude before γ-DGG attenuation, and an equal proportion of events were then compared after drug application to determine mean attenuation (consistent probability of release was assumed). Traces for which access resistance varied substantially or were > 25 MΩ were rejected from analysis. Image analysis was carried out via custom scripts written in ImagePro Plus (Media Cybernetics, Carlsbad, CA) for puncta localization and quantification. Pixels within each punctum were assigned intensity values, and the combined sum of a punctum's intensity values, or integrated optical density, was taken as the punctum's total intensity. VGLUT1 total intensity was measured against that of synapsin I or synaptotagmin in the same punctum. All comparisons involving multiple conditions were quantified first using ANOVA, followed by unpaired t-tests between adjacent groups as reported, and all error bars report standard mean error unless otherwise noted.

Micropattern Fabrication

AutoCAD software from Designers' CADD Company, Inc. was used to create a micropattern of increasingly larger squares which were repeated over three rows. The photomask was custom printed by Advance Reproductions Corporation onto a transparency and transferred, via UV exposure and developing, onto silicon wafers which were covered in a thin layer of photoresist (Silicone Sense, Incorporated). The resulting features of the photoresist were used as a mold to create a microstamp. For this segment in the fabrication process, poly(dimehylsiloxane) PDMS was purchased from Dow Chemical Company, and it was poured onto the silicone wafer and cured with heat. The PDMS was consequently peeled from the wafer and thereby contained the geometric features of squares originally described.

An electron-beam evaporator at the Whitehead Institute was used to deposit a thin layer of gold and titanium onto the surface of a glass coverslip (Titanium was Cat. No.43367-5 and gold was Cat. No. 37316-8; both were from Sigma-Aldrich). This coverslip was used as the solid substrate upon which the microstamp was put in contact. That is, the PDMS stamp was "inked" with hydrophobic alkanethiols (purchased and

purified before use), dried with nitrogen gas, and brought into tight contact with the surface of the coverslip. Consequently, the hydrophobic alkanethiol molecules were transferred onto to the regions of the glass surface that only contacted the raised regions of the stamp. Once the alkanethiols were transferred to the gold surface, they immediately formed self assembled monolayers limited to the square islands.

Chemicals as well as the synthesis of nonadhesive alkanethiol SAMs were supplied by the Whitesides lab. They included (tridecafluor-1,1,2,2-tetrahydrooctyl)-1-trichlorosilane, tetrahydrofuran, deuterated chloroform, 11-brmoundec-1-ene, calcium hydride, hexadecanethiol, hexanes, sodium hydroxide, benzophenone, dichloromethane, sodium sulfate, recrystallized 2,2'-azobisisobutyronitrile, thiolacetic acid, sodium methoxide, tri(ethylene glycol), and DL-camphor-10-sulfonic acid. Other common basic laboratory equipment and materials (e.g., thin-layer chromatography, column chromatography, nuclear magnetic resonance, 450-W medium-pressure mercury lamp, ace glass, rotary evaporator) were also supplied by the Whitesides group. The nonadhesive alkanethiolate, (1-mercaptoundec-11-yl)tri(ethylene glycol), was created by first combining (undec-1-en-1-yl)tri(ethyleneglycol) with sodium hydroxide, tri(ethylene glycol), and 11-bromoundec-1-ene. This product was then purified and used to synthesize {1-[(methylcarbonyl)thio] undec-11yl}tri(ethylene glycol), and eventually the final nonadhesive product.

After a few minutes to allow permanent stabilization of the adhesive SAMs, a solution containing the nonadhesive poly(ethylene glycol)-alkanethiolate (PEG), which contains terminal triethylene glycol groups was added. The nonadhesive alkanethiol similarly formed a SAM between the adhesive regions, and a continuous SAM was thereby formed over the entire glass surface. Just before deposition of primary cell culture of hippocampal neurons, a solution of laminin at 50 □g/ml was used to coat the square islands, as only the hydrophobic surfaces allowed physiosorption of protein. The PEG covered nonadhesive regions remained free of laminin in addition to repelling any extracellular matrix deposition by neurons themselves. When hippocampal neurons were plated onto the laminin coated micropatterned substrates, they preferentially attached to the islands and spread to assume the island's size and shape.

REFERENCES

Aravanis AM, Pyle JL, Tsien RW (2003) Single synaptic vesicles fusing transiently and successively without loss of identity. Nature 423:643-647.

Atwood HL, Karunanithi S (2002) Diversification of synaptic strength: presynaptic elements. Nat Rev Neurosci 3:497-516.

Auger C, Marty A (2000) Quantal currents at single-site central synapses. J Physiol 526 Pt 1:3-11.

Balice-Gordon RJ, Lichtman JW (1993) In vivo observations of pre- and postsynaptic changes during the transition from multiple to single innervation at developing neuromuscular junctions. J Neurosci 13:834-855.

Balice-Gordon RJ, Lichtman JW (1994) Long-term synapse loss induced by focal blockade of postsynaptic receptors. Nature 372:519-524.

Bekkers JM, Richerson GB, Stevens CF (1990) Origin of variability in quantal size in cultured hippocampal neurons and hippocampal slices. Proc Natl Acad Sci U S A 87:5359-5362.

Bellocchio EE, Reimer RJ, Fremeau RT, Jr., Edwards RH (2000) Uptake of glutamate into synaptic vesicles by an inorganic phosphate transporter. Science 289:957-960.

Betz WJ, Bewick GS (1992) Optical analysis of synaptic vesicle recycling at the frog neuromuscular junction. Science 255:200-203.

Bi GQ, Poo MM (1998) Synaptic modifications in cultured hippocampal neurons: dependence on spike timing, synaptic strength, and postsynaptic cell type. J Neurosci 18:10464-10472.

Bruns D, Riedel D, Klingauf J, Jahn R (2000) Quantal release of serotonin. Neuron 28:205-220.

Burrone J, O'Byrne M, Murthy VN (2002) Multiple forms of synaptic plasticity triggered by selective suppression of activity in individual neurons. Nature 420:414-418.

Busetto G, Buffelli M, Tognana E, Bellico F, Cangiano A (2000) Hebbian mechanisms revealed by electrical stimulation at developing rat neuromuscular junctions. J Neurosci 20:685-695.

Chapman B, Jacobson MD, Reiter HO, Stryker MP (1986) Ocular dominance shift in kitten visual cortex caused by imbalance in retinal electrical activity. Nature 324:154-156.

Colliver TL, Pyott SJ, Achalabun M, Ewing AG (2000) VMAT-Mediated changes in quantal size and vesicular volume. J Neurosci 20:5276-5282.

Colman H, Nabekura J, Lichtman JW (1997) Alterations in synaptic strength preceding axon withdrawal. Science 275:356-361.

Culican SM, Nelson CC, Lichtman JW (1998) Axon withdrawal during synapse elimination at the neuromuscular junction is accompanied by disassembly of the postsynaptic specialization and withdrawal of Schwann cell processes. J Neurosci 18:4953-4965.

Fagiolini M, Hensch TK (2000) Inhibitory threshold for critical-period activation in primary visual cortex. Nature 404:183-186.

Fonseca R, Nagerl UV, Morris RG, Bonhoeffer T (2004) Competing for memory: hippocampal LTP under regimes of reduced protein synthesis. Neuron 44:1011-1020.

Forti L, Bossi M, Bergamaschi A, Villa A, Malgaroli A (1997) Loose-patch recordings of single quanta at individual hippocampal synapses. Nature 388:874-878.
Franks KM, Stevens CF, Sejnowski TJ (2003) Independent sources of quantal variability at single glutamatergic synapses. J Neurosci 23:3186-3195.
Fremeau RT, Troyer MD, Pahner I, Nygaard GO, Tran CH, Reimer RJ, Bellocchio EE, Fortin D, Storm-Mathisen J, Edwards RH (2001) The expression of vesicular glutamate transporters defines two classes of excitatory synapse. Neuron 31:247-260.
Fremeau RT, Jr., Kam K, Qureshi T, Johnson J, Copenhagen DR, Storm-Mathisen J, Chaudhry FA, Nicoll RA, Edwards RH (2004) Vesicular glutamate transporters 1 and 2 target to functionally distinct synaptic release sites. Science 304:1815-1819.
Fremeau RT, Jr., Burman J, Qureshi T, Tran CH, Proctor J, Johnson J, Zhang H, Sulzer D, Copenhagen DR, Storm-Mathisen J, Reimer RJ, Chaudhry FA, Edwards RH (2002) The identification of vesicular glutamate transporter 3 suggests novel modes of signaling by glutamate. Proc Natl Acad Sci U S A 99:14488-14493.
Gandhi SP, Stevens CF (2003) Three modes of synaptic vesicular recycling revealed by single-vesicle imaging. Nature 423:607-613.
Hahm JO, Langdon RB, Sur M (1991) Disruption of retinogeniculate afferent segregation by antagonists to NMDA receptors. Nature 351:568-570.
Hanse E, Gustafsson B (2001) Quantal variability at glutamatergic synapses in area CA1 of the rat neonatal hippocampus. J Physiol 531:467-480.
Harris KM, Stevens JK (1989) Dendritic spines of CA 1 pyramidal cells in the rat hippocampus: serial electron microscopy with reference to their biophysical characteristics. J Neurosci 9:2982-2997.
Hell JW, Maycox PR, Stadler H, Jahn R (1988) Uptake of GABA by rat brain synaptic vesicles isolated by a new procedure. Embo J 7:3023-3029.
Ishikawa T, Sahara Y, Takahashi T (2002) A single packet of transmitter does not saturate postsynaptic glutamate receptors. Neuron 34:613-621.
Jansen JK, Fladby T (1990) The perinatal reorganization of the innervation of skeletal muscle in mammals. Prog Neurobiol 34:39-90.
Jin H, Wu H, Osterhaus G, Wei J, Davis K, Sha D, Floor E, Hsu CC, Kopke RD, Wu JY (2003) Demonstration of functional coupling between gamma -aminobutyric acid (GABA) synthesis and vesicular GABA transport into synaptic vesicles. Proc Natl Acad Sci U S A 100:4293-4298.
Karunanithi S, Marin L, Wong K, Atwood HL (2002) Quantal size and variation determined by vesicle size in normal and mutant Drosophila glutamatergic synapses. J Neurosci 22:10267-10276.
Liu G (2003) Presynaptic control of quantal size: kinetic mechanisms and implications for synaptic transmission and plasticity. Curr Opin Neurobiol 13:324-331.
Liu G (2004) Local structural balance and functional interaction of excitatory and inhibitory synapses in hippocampal dendrites. Nat Neurosci 7:373-379.
Liu G, Tsien RW (1995) Properties of synaptic transmission at single hippocampal synaptic boutons. Nature 375:404-408.
Liu G, Choi S, Tsien RW (1999) Variability of neurotransmitter concentration and nonsaturation of postsynaptic AMPA receptors at synapses in hippocampal cultures and slices. Neuron 22:395-409.
Mainen ZF, Malinow R, Svoboda K (1999) Synaptic calcium transients in single spines indicate that NMDA receptors are not saturated. Nature 399:151-155.

Malenka RC, Nicoll RA (1999) Long-term potentiation--a decade of progress? Science 285:1870-1874.
Maycox PR, Deckwerth T, Hell JW, Jahn R (1988) Glutamate uptake by brain synaptic vesicles. Energy dependence of transport and functional reconstitution in proteoliposomes. J Biol Chem 263:15423-15428.
McAllister AK, Stevens CF (2000) Nonsaturation of AMPA and NMDA receptors at hippocampal synapses. Proc Natl Acad Sci U S A 97:6173-6178.
Murthy VN, Stevens CF (1998) Synaptic vesicles retain their identity through the endocytic cycle. Nature 392:497-501.
Murthy VN, Sejnowski TJ, Stevens CF (1997) Heterogeneous release properties of visualized individual hippocampal synapses. Neuron 18:599-612.
Murthy VN, Schikorski T, Stevens CF, Zhu Y (2001) Inactivity produces increases in neurotransmitter release and synapse size. Neuron 32:673-682.
Nelson S, Toth L, Sheth B, Sur M (1994) Orientation selectivity of cortical neurons during intracellular blockade of inhibition. Science 265:774-777.
Ni B, Rosteck PR, Jr., Nadi NS, Paul SM (1994) Cloning and expression of a cDNA encoding a brain-specific Na(+)-dependent inorganic phosphate cotransporter. Proc Natl Acad Sci U S A 91:5607-5611.
O'Brien RJ, Kamboj S, Ehlers MD, Rosen KR, Fischbach GD, Huganir RL (1998) Activity-dependent modulation of synaptic AMPA receptor accumulation. Neuron 21:1067-1078.
Oertner TG, Sabatini BL, Nimchinsky EA, Svoboda K (2002) Facilitation at single synapses probed with optical quantal analysis. Nat Neurosci 5:657-664.
Ogita K, Hirata K, Bole DG, Yoshida S, Tamura Y, Leckenby AM, Ueda T (2001) Inhibition of vesicular glutamate storage and exocytotic release by Rose Bengal. J Neurochem 77:34-42.
Pierce JP, Lewin GR (1994) An ultrastructural size principle. Neuroscience 58:441-446.
Pothos EN, Larsen KE, Krantz DE, Liu Y, Haycock JW, Setlik W, Gershon MD, Edwards RH, Sulzer D (2000) Synaptic vesicle transporter expression regulates vesicle phenotype and quantal size. J Neurosci 20:7297-7306.
Pratt KG, Watt AJ, Griffith LC, Nelson SB, Turrigiano GG (2003) Activity-dependent remodeling of presynaptic inputs by postsynaptic expression of activated CaMKII. Neuron 39:269-281.
Purves D, Lichtman JW (1980) Elimination of synapses in the developing nervous system. Science 210:153-157.
Rankin CH, Wicks SR (1995) Mutations of the *Caenorhabditis elegans* Brain-Specific Inorganic Phosphate Transporter *eat-4* Affect Habituation of the Tap-Withdrawal Response without Affecting the Response Itself. J Neurosci 15:2434-2444.
Renger JJ, Egles C, Liu G (2001) A developmental switch in neurotransmitter flux enhances synaptic efficacy by affecting AMPA receptor activation. Neuron 29:469-484.
Rose JK, Kaun KR, Rankin CH (2002) A new group-training procedure for habituation demonstrates that presynaptic glutamate release contributes to long-term memory in Caenorhabditis elegans. Learn Mem 9:130-137.
Roseth S, Fykse EM, Fonnum F (1998) Uptake of L-glutamate into synaptic vesicles: competitive inhibition by dyes with biphenyl and amino- and sulphonic acid-substituted naphthyl groups. Biochem Pharmacol 56:1243-1249.
Ryan TA, Smith SJ, Reuter H (1996) The timing of synaptic vesicle endocytosis. Proc Natl Acad Sci U S A 93:5567-5571.

Sala C, Piech V, Wilson NR, Passafaro M, Liu G, Sheng M (2001) Regulation of dendritic spine morphology and synaptic function by Shank and Homer. Neuron 31:115-130.

Schafer MK, Varoqui H, Defamie N, Weihe E, Erickson JD (2002) Molecular cloning and functional identification of mouse vesicular glutamate transporter 3 and its expression in subsets of novel excitatory neurons. J Biol Chem 277:50734-50748.

Schikorski T, Stevens CF (1997) Quantitative ultrastructural analysis of hippocampal excitatory synapses. J Neurosci 17:5858-5867.

Sheng M, Kim MJ (2002) Postsynaptic signaling and plasticity mechanisms. Science 298:776-780.

Silver RA, Cull-Candy SG, Takahashi T (1996) Non-NMDA glutamate receptor occupancy and open probability at a rat cerebellar synapse with single and multiple release sites. J Physiol 494 (Pt 1):231-250.

Sin WC, Haas K, Ruthazer ES, Cline HT (2002) Dendrite growth increased by visual activity requires NMDA receptor and Rho GTPases. Nature 419:475-480.

Slutsky I, Sadeghpour S, Li B, Liu G (2004) Enhancement of synaptic plasticity through chronically reduced Ca2+ flux during uncorrelated activity. Neuron 44:835-849.

Song H, Ming G, Fon E, Bellocchio E, Edwards RH, Poo M (1997) Expression of a putative vesicular acetylcholine transporter facilitates quantal transmitter packaging. Neuron 18:815-826.

Stryker MP, Harris WA (1986) Binocular impulse blockade prevents the formation of ocular dominance columns in cat visual cortex. J Neurosci 6:2117-2133.

Sulzer D, Pothos EN (2000) Regulation of quantal size by presynaptic mechanisms. Rev Neurosci 11:159-212.

Sulzer D, Edwards R (2000) Vesicles: equal in neurotransmitter concentration but not in volume. Neuron 28:5-7.

Takamori S, Rhee JS, Rosenmund C, Jahn R (2000) Identification of a vesicular glutamate transporter that defines a glutamatergic phenotype in neurons. Nature 407:189-194.

Takamori S, Rhee JS, Rosenmund C, Jahn R (2001) Identification of differentiation-associated brain-specific phosphate transporter as a second vesicular glutamate transporter (VGLUT2). J Neurosci 21:RC182.

Takamori S, Malherbe P, Broger C, Jahn R (2002) Molecular cloning and functional characterization of human vesicular glutamate transporter 3. EMBO Rep 3:798-803.

Thiagarajan TC, Piedras-Renteria ES, Tsien RW (2002) alpha- and betaCaMKII. Inverse regulation by neuronal activity and opposing effects on synaptic strength. Neuron 36:1103-1114.

Tong G, Jahr CE (1994) Multivesicular release from excitatory synapses of cultured hippocampal neurons. Neuron 12:51-59.

Turrigiano GG, Nelson SB (2000) Hebb and homeostasis in neuronal plasticity. Curr Opin Neurobiol 10:358-364.

Turrigiano GG, Leslie KR, Desai NS, Rutherford LC, Nelson SB (1998) Activity-dependent scaling of quantal amplitude in neocortical neurons. Nature 391:892-896.

Varoqui H, Schafer MK, Zhu H, Weihe E, Erickson JD (2002) Identification of the differentiation-associated Na+/PI transporter as a novel vesicular glutamate transporter expressed in a distinct set of glutamatergic synapses. J Neurosci 22:142-155.

Wadiche JI, Jahr CE (2001) Multivesicular release at climbing fiber-Purkinje cell synapses. Neuron 32:301-313.
Watt AJ, van Rossum MC, MacLeod KM, Nelson SB, Turrigiano GG (2000) Activity coregulates quantal AMPA and NMDA currents at neocortical synapses. Neuron 26:659-670.
Weliky M, Katz LC (1997) Disruption of orientation tuning in visual cortex by artificially correlated neuronal activity. Nature 386:680-685.
Wierenga CJ, Ibata K, Turrigiano GG (2005) Postsynaptic expression of homeostatic plasticity at neocortical synapses. J Neurosci 25:2895-2905.
Wiesel TN (1982) Postnatal development of the visual cortex and the influence of environment. Nature 299:583-591.
Wojcik SM, Rhee JS, Herzog E, Sigler A, Jahn R, Takamori S, Brose N, Rosenmund C (2004) An essential role for vesicular glutamate transporter 1 (VGLUT1) in postnatal development and control of quantal size. Proc Natl Acad Sci U S A 101:7158-7163.
Wolosker H, de Souza DO, de Meis L (1996) Regulation of glutamate transport into synaptic vesicles by chloride and proton gradient. J Biol Chem 271:11726-11731.
Yamashita T, Ishikawa T, Takahashi T (2003) Developmental increase in vesicular glutamate content does not cause saturation of AMPA receptors at the calyx of held synapse. J Neurosci 23:3633-3638.
Zhou Q, Petersen CC, Nicoll RA (2000) Effects of reduced vesicular filling on synaptic transmission in rat hippocampal neurones. J Physiol 525:195-206.